SUPERVISED DISENTANGLEMENT UNDER HIDDEN CORRELATIONS

Anonymous authors
Paper under double-blind review

ABSTRACT

Disentangled representation learning (DRL) methods are often leveraged to improve the generalization of representations. Recent DRL methods have tried to handle attribute correlations by enforcing conditional independence based on attributes. However, the complex multi-modal data distributions and hidden correlations under attributes remain unexplored. Existing methods are theoretically shown to cause the loss of mode information under such hidden correlations. To solve this problem, we propose Supervised Disentanglement under Hidden Correlations (SD-HC), which discovers data modes under certain attributes and minimizes mode-based conditional mutual information to achieve disentanglement. Theoretically, we prove that SD-HC is sufficient for disentanglement under hidden correlations, preserving mode information and attribute information. Empirically, extensive experiments on one toy dataset and five real-world datasets demonstrate improved generalization against the state-of-the-art baselines. Codes are available at anonymous Github `https://anonymous.4open.science/r/SD-HC`.

1 INTRODUCTION

Disentangled representation learning (DRL) aims to encode one single data attribute in each representation subspace, which holds great promise in enhancing generalization to unseen scenarios (Matthes et al., 2023; Qian et al., 2021), enabling controllable generative modeling (Yuan et al., 2021), and improving fairness (Locatello et al., 2019a). In the supervised setting, each representation subspace is learned under the label supervision of its corresponding attribute, while being disentangled from other attributes.

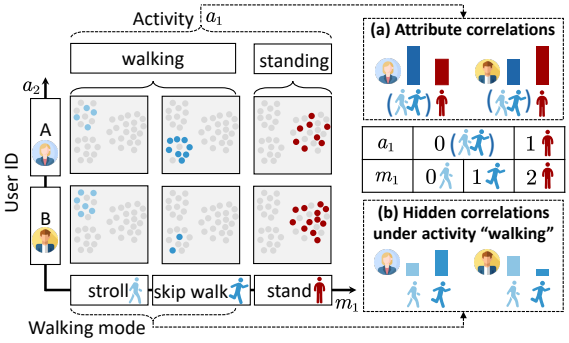

Figure 1: Correlated human activity data. The distributions of (a) **"walking" / "standing"**, and (b) **"stroll" / "skip walk"** under "walking" differ between users, exhibiting correlations.

Supervised DRL methods typically assume independence between attributes. In addition to supervised prediction, mutual information (MI) minimization (Kwon et al., 2020; Yuan et al., 2021; Su et al., 2022) is commonly adopted to enforce independence between the representations of different attributes and achieve disentanglement. The independence assumption is often violated in real-world data, where correlations are prevalent. Taking human activities as an example, different users have different behavior patterns, and each user tends to engage in some activities more frequently than others, exhibiting correlations between activity and user identity (ID) attributes, as shown in Figure 1a. For correlated attributes, enforcing representation independence causes at least one subspace to lose attribute-related information (Funke et al., 2022).

To disentangle correlated attributes, attribute-based conditional mutual information minimization (A-CMI) (Funke et al., 2022) enforces conditional representation independence that preserves attribute-related information. However, when a certain attribute takes a value, underlying variations related to this attribute may lead to complex multi-modal data distributions rather than simple uni-modal

data distributions. The mode under this value of this attribute may be correlated with other attributes. Continuing with the human activity example, when activity attribute takes the value "walking", variations in pace, stride, and posture may lead to different walking modes, the casual "stroll" and energetic "skip walk"; different users have more subtle differences in their behavior patterns, exhibiting correlations between walking mode and user ID attribute, as shown in Figure 1b. In this case, A-CMI may cause the loss of mode information (as proved in Proposition 1), which is important for attribute prediction with multi-modality (Nie et al., 2020; Sugiyama, 2021; Li et al., 2017). For example, in human activity recognition, losing the information about walking modes might lead to the confusion between "skip walk" and another activity "climbing down", while encoding mode information can better distinguish these similar activities.

To address the above problem, we propose Supervised Disentanglement under Hidden Correlations (SD-HC). Instead of focusing on attribute correlations as existing works, we delve into the complex data distributions and hidden correlations under certain attributes. Our contributions are:

- We introduce a novel supervised DRL paradigm named SD-HC, which discovers data modes under certain attributes and disentangles these attributes with mode-based CMI minimization. Under hidden correlations, SD-HC can preserve mode information that current methods tend to lose.
- We theoretically prove that mode-based CMI minimization is the *necessary and sufficient condition* for supervised disentanglement under both hidden correlations and attribute correlations. This result can be extended to show that CMI minimization can achieve disentanglement under correlations in general, establishing the first *sufficient condition* for disentanglement under correlations.
- We extensively evaluate SD-HC on five real-world datasets, which demonstrates that SD-HC outperforms the state-of-the-art DRL methods for attribute prediction on out-of-distribution data and data under train-test correlation shifts. We conduct comprehensive investigations on toy data and real-world data regarding the behavior of different methods, the impact of train correlation strength, noise level, train-test correlation shifts, and the learned representations, which demonstrate the superiority of SD-HC under various circumstances.

2 Related Work

Disentanged Representation Learning DRL methods can be roughly divided into unsupervised, weakly-supervised, and supervised DRL. Unsupervised DRL learns independent representation dimensions that each correspond to an unknown attribute by self-supervised tasks, e.g., self-reconstruction in variational auto-encoders (VAEs) (Higgins et al., 2016; Kim & Mnih, 2018; Chen et al., 2018) or contrastive learning (Zimmermann et al., 2021; Matthes et al., 2023). Yet, the feasibility of purely unsupervised disentanglement has been questioned (Locatello et al., 2019b), which prompts DRL with weak supervision (Shu et al., 2020), e.g., similarity (Chen & Batmanghelich, 2020) or grouping information (Bouchacourt et al., 2018). In contrast, supervised DRL learns individual multi-dimensional representation subspaces that each encode an attribute under label supervision (Qian et al., 2021; Yuan et al., 2021). Generally, DRL methods assume attribute independence and enforce representation independence between different attributes as a means of disentanglement. In particular, supervised DRL usually minimizes the MI between attribute representations (Kwon et al., 2020; Yuan et al., 2021; Su et al., 2022), minimizes the Maximum Mean Discrepancy (MMD) between representation distributions (Li et al., 2018; Lin et al., 2020), or makes one attribute unpredictable from the representations of another by adversarial training (Qian et al., 2021; Li et al., 2022; Lee et al., 2021). Our work falls under supervised DRL.

Disentanglement Under Attribute Correlations Recent works have revealed that independence assumption-based DRL fails on correlated attributes, where independence constraints cause entanglement for unsupervised DRL (i.e., one dimension encodes two or more correlated attributes) (Träuble et al., 2021) or hurt the predictive ability of representations for supervised DRL (Funke et al., 2022). To disentangle correlated attributes for unsupervised DRL, Träuble et al. (Träuble et al., 2021) and Dittadi et al. (Dittadi et al., 2021) add weak supervision or a few labels to correct the model. Differently, Wang et al. (Wang & Jordan, 2021) and Roth et al. (Roth et al., 2023) relax independence constraints with Hausdorff distance to encourage only factorized supports instead of

factorized distributions. These methods can somewhat alleviate entanglement but do not guarantee disentanglement theoretically (Funke et al., 2022; Wang & Jordan, 2021).

More recent works have introduced conditional independence constraints to disentangle correlated attributes. For supervised DRL, Funke et al. (Funke et al., 2022) introduces attribute-based CMI minimization (A-CMI). For each attribute, A-CMI minimizes the MI conditioned on this attribute between its representation and the joint representations of all other attributes. A-CMI is proved to be the *necessary* condition for disentanglement under attribute correlations, whereas unconditional MI is proved to fail. For unsupervised DRL in reinforcement learning, Dunion et al. (Dunion et al., 2023) follow A-CMI, but condition on history information to make up for the unknown current values.

To the best of our knowledge, existing works have only established *necessary* conditions for disentangling correlated attributes (Wang & Jordan, 2021; Funke et al., 2022), and the sufficiency of CMI has only been validated on linear regression examples rather than proved theoretically. We are the first to give *sufficient* conditions for disentanglement under correlations, theoretically proving that CMI minimization can achieve disentanglement. Our results hold under various cases, including multiple attributes under attribute correlations and hidden correlations.

3 Disentanglement under Hidden Correlations

3.1 Problem Formulation

Data Generation Process. We assume that data are generated from the causal process in Definition 1 and Figure 2, which mainly relies on the *independent mechanism assumption* (Schölkopf et al., 2012) that attributes are casually independent, i.e., each attribute arises on its own, allowing changes or interventions on one attribute without affecting others. Still, confounding may exist.

Definition 1. (Disentangled Causal Process). *Consider a causal generative model $p(\boldsymbol{x}|\boldsymbol{a})$ for data $\boldsymbol{x}$ with K attributes $\boldsymbol{a} = (a_1, a_2, ..., a_K)$. A certain attribute a_k is associated with a categorical mode variable m_k. Attributes $\boldsymbol{a}$ could be influenced by L confounders $\boldsymbol{c}^a = (c_1^a, ..., c_L^a)$. Conditioned on a_k, mode variable m_k and other attributes $\boldsymbol{a}_{-k}$ could be influenced by Q confounders $\boldsymbol{c}^m = (c_1^m, ..., c_Q^m)$. This causal model is called disentangled if and only if it can be described by a structural causal model (SCM) (Pearl, 2009) of the form:*

$$
\begin{aligned}
\boldsymbol{c}^a &\leftarrow \boldsymbol{n}^{ca}, \boldsymbol{c}^m \leftarrow \boldsymbol{n}^{cm} \\
a_k &\leftarrow h_k^a(S_k^a, \boldsymbol{n}_k^a), S_k^a \subset \{c_1^a, ..., c_L^a\}, k \in \{1, ..., K\} \\
a_j &\leftarrow h_j^a(S_j^a, S_j^m, \boldsymbol{n}_j^a), S_j^a \subset \{c_1^a, ..., c_L^a\}, S_j^m \subset \{c_1^m, ..., c_Q^m\}, j \neq k \\
m_k &\leftarrow h^m(a_k, \boldsymbol{c}^m, \boldsymbol{n}^m) \\
\boldsymbol{x} &\leftarrow g(\boldsymbol{a}_{-k}, m_k, \boldsymbol{n}^x)
\end{aligned}
\tag{1}
$$

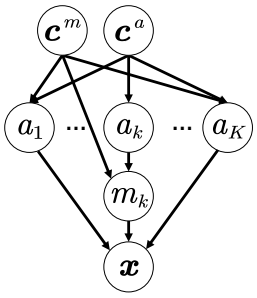

Figure 2: Causal graph of data generation with multi-modality and hidden correlations under a certain a_k.

with functions g, h_i^a, h^m, jointly independent noise variables $\boldsymbol{n}^{ca}$, $\boldsymbol{n}^{cm}$, $\boldsymbol{n}_i^a$, $\boldsymbol{n}^m$, $\boldsymbol{n}^x$, and confounder subsets S_i^a, S_j^m, for $i = 1, ..., K$, $j = 1, ..., k-1, k+1, ..., K$. $-k$ denotes the set of attribute indices $\{j\}_{j \neq k}$. Note that $\forall i \neq i', a_i \not\rightarrow a_{i'}$.

Correlations. We denote mutual information (MI) and entropy function as $I(\cdot;\cdot)$ and $H(\cdot)$, respectively. The MI between attributes measures their correlations, e.g., $I(a_i; a_{i'}), i \neq i'$, while the MI between a representation and an attribute measures the amount of information the representation contains about the attribute, e.g., $I(\boldsymbol{z}_i; a_{i'})$. We denote attribute correlations as $I(a_i; a_{i'})$ and hidden correlations as $I(m_k; a_{-k}|a_k)$, which are induced by confounders $\boldsymbol{c}^a$ and $\boldsymbol{c}^m$, respectively.

Multi-Modality and Hidden Correlations. Under some value α of a_k, the data distribution is assumed to be multi-modal due to underlying variations related to this attribute, i.e., $p(\boldsymbol{x}|a_k = \alpha)$ is a mixture model, e.g., Gaussian mixture model, and a mode corresponds to a component of the mixture. The modes under different attribute values are labeled altogether to formulate the categorical variable m_1, e.g., for a_k with 2 values ($|\mathcal{A}_k| = 2$) and 3 modes under each value, the 6 modes in total will be labeled from 0 to 5 to formulate m_1. The modes under $a_k = \alpha$ may be correlated with other attributes a_{-k}, i.e., $I(m_k; a_{-k}|a_k = \alpha) > 0$. Hidden correlations are defined as the expectation over different attribute values, i.e., $I(m_k; a_{-k}|a_k) = \sum_{\alpha \in \mathcal{A}_k} p_{a_k}(a_k = \alpha) I(m_k; a_{-k}|a_k = \alpha)$.

Intuitive Example. Figure 1 illustrates hidden correlations in the realistic application of human activity recognition: Under different values of activity attribute a_1, two walking modes and one standing mode are labeled altogether to formulate variable m_1, i.e., $m_1 = 0, 1, 2$ indicates "stroll", "skip walk", and "stand", respectively; The modes "stroll" and "skip walk" under "walking" activity might be correlated with user ID attribute a_2, i.e., $I(m_1; a_2|a_1 = 0) > 0$, where $a_1 = 0$ indicates "walking" activity and $m_1|a_1 = 0$ indicates walking modes $m_1 = 0, 1$. For activity recognition, the goal is to learn disentangled activity representations that fully capture the activity and its modes, while remaining unaffected by personalized user patterns.

3.2 The Definitions of Disentangled Representations

The goal of supervised DRL is to learn disentangled representations $\boldsymbol{z}_i$ for each attribute a_i by a mapping $f(\boldsymbol{x}) = \boldsymbol{z} = (\boldsymbol{z}_1, \boldsymbol{z}_2, ..., \boldsymbol{z}_K), \boldsymbol{z}_i \in \mathbb{R}^D, i = 1, ..., K$. Disentangled $\boldsymbol{z}_i$ should (1) contain all information about a_i (***Informativeness***), which includes mode information for attributes with multi-modality, and (2) reflect the *causal independence* between attributes, such that external interventions by changing another attribute $a_j (i \neq j)$ alone should not affect $\boldsymbol{z}_i$ (***Independence***), which is formalized in Definition 2 following (Wang & Jordan, 2021; Suter et al., 2019).

Definition 2. (Disentangled Representation). *Representation $\boldsymbol{z}$ is disentangled, if for $i = 1, ..., K$:*

$$p(\boldsymbol{z}_i|\mathrm{do}(a_{-i})) = p(\boldsymbol{z}_i) \tag{2}$$

where $-i$ indicates the set of attribute indices $\{j\}_{j\neq i}$, a_{-i} indicates the joint variable of $\{a_j\}_{j\neq i}$, and $\mathrm{do}(\cdot)$ operation sets the values of some attributes by external intervention and leaves other attributes unchanged. Such external intervention is isolated from the causal effects within the causal process.

3.3 Theoretical Guarantees for Disentangling with Mode-Based CMI Minimization

We focus on the disentanglement of a certain attribute with multi-modality, and show that under the *independent mechanism assumption*, mode-based CMI minimization is the necessary and sufficient condition for supervised disentanglement under hidden correlations and attribute correlations, while A-CMI fails under hidden correlations. For simplicity, we take $K = 2$ as an example, with a_1 exhibiting multi-modality. Then, the results are generalized to multiple attributes and simple cases.

The Necessary Condition for Disentanglement. Based on the data generation process of Definition 1, we build the causal graphs of the true latent representations (denoted as $\boldsymbol{z}_k^l$), which are only causally dependent on the corresponding attribute or mode, and are inherently disentangled.

Since the ideally disentangled $\boldsymbol{z}_k$ should capture the true latent $\boldsymbol{z}_k^l$ and retain its properties, we find conditional independence between the true latent representations as the necessary condition for disentanglement. As stated by the causal graph theorems in Appendix C, two variables X, Y are conditionally independent given a variable that blocks all *backdoor paths* between them, i.e., the paths that flow backward from X or Y. In Figure 3a, we consider only attribute correlations as A-CMI, where a_1 blocks the only *backdoor path* between $\boldsymbol{z}_1^l$ and $\boldsymbol{z}_2^l$. In comparison, we consider hidden correlations and potential attribute correlations in Figure 3b, where m_1 blocks all *backdoor paths* whether attribute correlations exist or not, yet a_1 fails to block the path containing $\boldsymbol{c}^m$. This means that under hidden correlations and potential attribute correlations, disentangled representations should retain the conditional independence of the true latent representations as:

$$I(\boldsymbol{z}_1^l; \boldsymbol{z}_2^l|m_1) = 0 \quad \Rightarrow \quad I(\boldsymbol{z}_1; \boldsymbol{z}_2|m_1) = 0 \tag{3}$$

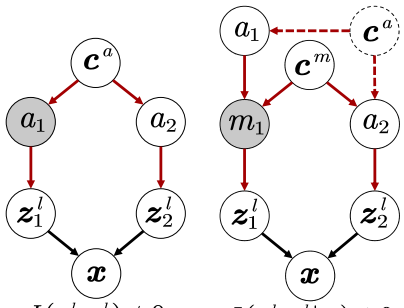

(a) A-CMI (b) SD-HC (ours)

Figure 3: Causal graphs of the true latent representations. **Red** arrows indicate the *backdoor paths* between $\boldsymbol{z}_1^l$ and $\boldsymbol{z}_2^l$. The dashed circle and arrows indicate that attribute correlations may or may not exist.

A-CMI Fails Under Hidden Correlations. As shown in Figure 3b, disentangled representations $\boldsymbol{z}_1$ and $\boldsymbol{z}_2$ are not conditionally independent given a_1 under hidden correlations. We further show that

enforcing such conditional independence could hurt the predictive ability of representations, which is formalized in Proposition 1 and proved in Appendix B.2.

Proposition 1. *For representations $\boldsymbol{z}_1, \boldsymbol{z}_2$ of m_1, a_2, respectively, if $I(m_1; a_2|a_1) > 0$, then enforcing $I(\boldsymbol{z}_1; \boldsymbol{z}_2|a_1) = 0$ leads to at least one of $I(\boldsymbol{z}_1; m_1) < H(m_1)$ and $I(\boldsymbol{z}_2; a_2) < H(a_2)$.*

where $I(\boldsymbol{z}_1; m_1) < H(m_1)$ indicates that $\boldsymbol{z}_1$ fails to contain mode information for predicting a_1, and $I(\boldsymbol{z}_2; a_2) < H(a_2)$ indicates that $\boldsymbol{z}_2$ fails to contain attribute-related information for predicting a_2. Either way, attribute-based CMI minimization $I(\boldsymbol{z}_1; \boldsymbol{z}_2|a_1) = 0$ hurts the predictive ability of representations under hidden correlations. This is an extension of Proposition 3.1 in (Funke et al., 2022), which proves that unconditional MI minimization fails under attribute correlations.

The Sufficient Condition for Disentanglement. Since inappropriate independence constraints could hurt the predictive ability of representations, the key to disentanglement is to find suitable independence constraints. We show that mode-based CMI minimization (Equation 3) is sufficient for supervised disentanglement under the *independent mechanism assumption* with various correlations.

For the two criteria of disentanglement: (1) ***Informativeness*** requires $I(\boldsymbol{z}_1; a_1) = H(a_1)$ and $I(\boldsymbol{z}_1; m_1) = H(m_1)$, which can be achieved by cross-entropy minimization (Boudiaf et al., 2020). Since mode-based CMI minimization has been proven necessary for disentanglement, it preserves the predictive ability of representations. (2) ***Independence*** is a bit tricky, as the impact of external interventions cannot be directly evaluated (Wang & Jordan, 2021). We prove that mode-based CMI minimization ensures representations are conditionally independent of other attributes (Proposition 2, Appendix B.3), and then prove that under the *independent mechanism assumption*, this conditional independence yields disentanglement as in Definition 2 (Proposition 3, Appendix B.3).

Proposition 2. *For representations $\boldsymbol{z}_1, \boldsymbol{z}_2$ of m_1, a_2, respectively, if $I(\boldsymbol{z}_1; m_1) = H(m_1)$, $I(\boldsymbol{z}_2; a_2) = H(a_2)$, and $I(\boldsymbol{z}_1; \boldsymbol{z}_2|m_1) = 0$, then $I(\boldsymbol{z}_1; a_2) = I(m_1; a_2)$ and $I(\boldsymbol{z}_1; a_2|m_1) = 0$.*

where $I(m_1; a_2)$ is denoted as the *total hidden correlations* between m_1 and a_2. As proved in Appendix B.1, total hidden correlations are the sum of attribute correlations and hidden correlations, i.e., $I(m_1; a_2) = I(a_1; a_2) + I(m_1; a_2|a_1)$. Thereby, $I(\boldsymbol{z}_1; a_2) = I(m_1; a_2)$ shows that $\boldsymbol{z}_1$ contains information about a_2 only if it is induced by correlations regarding its attribute or mode. Furthermore, $I(\boldsymbol{z}_1; a_2|m_1) = 0$ shows that $\boldsymbol{z}_1$ contains no additional information about a_2 knowing its mode.

Proposition 3. *Under the data generation assumption of Definition 1 ($K = 2$, $k = 1$) with independent mechanisms, if $I(\boldsymbol{z}_1; a_2|m_1) = 0$ for representation $\boldsymbol{z}_1$, then $p(\boldsymbol{z}_1|\mathrm{do}(a_2)) = p(\boldsymbol{z}_1)$.*

This is proved by do-calculous (Pearl, 2009), linking to Definition 2 and completing our proof.

Generalization to Multiple Attributes and Simple Cases. Our theoretical results naturally generalize to (1) $K > 2$, where the extension mainly involves replacing single variables a_2, $\boldsymbol{z}_2$ with joint variables a_{-k}, $\boldsymbol{z}_{-k}$, as discussed in Appendix B.5; (2) simple uni-modal data with attribute correlations, where the number of modes under each attribute value reduces to 1, and mode-based CMI degrades to attribute-based CMI; and (3) simple uncorrelated data, where confounding can be neglected, and mode-based CMI performs similarly to attribute-based CMI, as shown in Figure 8cd.

Theoretical Contributions. We prove the sufficiency of CMI for disentanglement, while the work of A-CMI only validates CMI on linear regression examples without formal proof. *This is the first attempt to establish sufficient conditions for disentanglement under correlations*, unlike necessary conditions before (Wang & Jordan, 2021; Funke et al., 2022). Our results generalize to multiple attributes, various correlation types, and simple uni-modal and uncorrelated data, showing that one independence constraint is sufficient for the supervised disentanglement of one representation $\boldsymbol{z}_k$. Formally, under the *independent mechanism assumption* in Definition 1, given the label supervision of all attributes and modes, when the supervised losses on all attributes and modes are optimized, and the CMI of $\boldsymbol{z}_k$ ($I(\boldsymbol{z}_k; \boldsymbol{z}_{-k}|m_k)$ for multi-modal or $I(\boldsymbol{z}_k; \boldsymbol{z}_{-k}|a_k)$ for uni-modal cases) is minimized, the learned $\boldsymbol{z}_k$ is disentangled as in Definition 2. The detailed discussions are in Appendix B.5.

4 METHOD

Framework. We show the framework of SD-HC for disentangling a certain attribute a_k with hidden correlations in Figure 4, which consists of encoder F for learning representations $F(\boldsymbol{x}) = \boldsymbol{z} = (\boldsymbol{z}_1, \boldsymbol{z}_2, ..., \boldsymbol{z}_K)$, $\boldsymbol{z}_i \in \mathbb{R}^D$, $i = 1, ..., K$, predictors $\{C_i\}_{i=1}^K$ for predicting each attribute, predictor

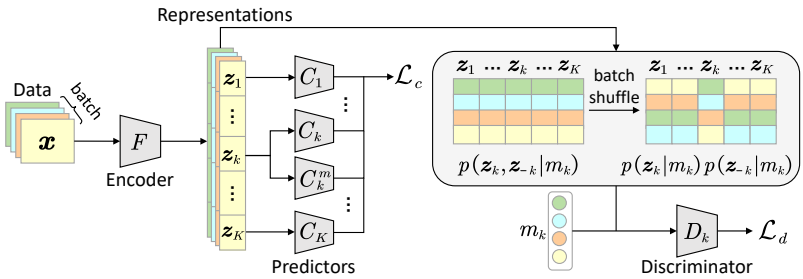

Figure 4: Framework of SD-HC for disentangling a certain $a_k, k \in \{1, ..., K\}$ with multi-modality.

C_k^m for predicting mode m_k, and discriminator D_k for minimizing mode-based CMI. SD-HC is architecture-agnostic and can be used in various applications.

The framework can be expanded to disentangle multiple attributes by adding one independence constraint to disentangle each attribute. The form of independence constraints depends on the correlation types, i.e., minimizing attribute-based CMI under attribute correlations or mode-based CMI under hidden correlations. Supervised constraints $I(\boldsymbol{z}_i; a_i) = H(a_i)$ are always required for $i = 1, ..., K$ with one additional constraint $I(\boldsymbol{z}_i; m_i) = H(m_i)$ for each attribute a_i with multi-modality. For additional constraints, discriminators and mode predictors should be added accordingly.

Mode Label Estimation. We assume the attribute labels are known, while the number of modes and the mode labels are unknown. To estimate mode labels for a_k, we perform clustering on the representations of a pre-trained encoder, which is trained with the supervised loss of a_k. Specifically, given the number of modes N_m, clustering is performed under each value of a_k, then the discovered modes under different values of a_k are labeled altogether to formulate m_k. We adopt k-means as the clustering method, which works well across our experiments. The numbers of modes N_m under different values of a_k are set to be equal and tuned as a hyper-parameter. We also provide practical guidance for different scenarios in Appendix I, including the alternative clustering methods and mode number estimation methods for reducing the computational costs of hyper-parameter tuning.

Losses. The losses are strictly designed according to the sufficient conditions for disentanglement. As commonly done in adversarial training (Chen et al., 2023), optimizations w.r.t. different losses are performed alternatively. The detailed training process is given in Appendix E.

(1) For supervised learning, attribute and mode prediction losses $\mathcal{L}_{ac}$, $\mathcal{L}_{mc}$ are formulated as:

$$\mathcal{L}_{ac} = \mathbb{E}_{\boldsymbol{x}}[\textstyle\sum_{k=1}^{K} l_{ce}(C_k(F_k(\boldsymbol{x})), a_k)] \ , \ \mathcal{L}_{mc} = \mathbb{E}_{\boldsymbol{x}}[l_{ce}(C_k^m(F_k(\boldsymbol{x})), m_k)] \tag{4}$$

$$\mathcal{L}_c = \mathcal{L}_{ac} + w_m \cdot \mathcal{L}_{mc} \tag{5}$$

where w_m is the weight of mode prediction loss, and $l_{ce}(\cdot)$ denotes cross entropy function.

(2) Since $I(\boldsymbol{z}_k; \boldsymbol{z}_{-k}|m_k) = 0$ if and only if $p(\boldsymbol{z}_k, \boldsymbol{z}_{-k}|m_k) = p(\boldsymbol{z}_k|m_k)p(\boldsymbol{z}_{-k}|m_k)$, we minimize CMI by matching the joint distribution $p(\boldsymbol{z}_k, \boldsymbol{z}_{-k}|m_k)$ with the marginal distribution $p(\boldsymbol{z}_k|m_k)p(\boldsymbol{z}_{-k}|m_k)$ with adversarial training (Belghazi et al., 2018). To sample from the two distributions, we loop over the values of mode labels $\mu \in \{0, ..., N_m * |\mathcal{A}_k| - 1\}$. For each value μ, we select the representations in the mini-batch with label $m_k = \mu$. The samples from the joint distribution are obtained by concatenating the selected representations, and those from the marginal distribution are obtained by shuffling the selected $\boldsymbol{z}_{-k}$ jointly then concatenating them with the selected $\boldsymbol{z}_k$. Jensen-Shannon Divergence is used to measure the discrepancy between the two distributions for stability (Hjelm et al., 2019). Discrimination loss $\mathcal{L}_d$ is formulated as follows, where $l_{bce}(\cdot)$ denotes binary cross entropy function:

$$\mathcal{L}_d = \mathbb{E}_{m_k}[\mathbb{E}_{(\boldsymbol{z}_k, \boldsymbol{z}_{-k})|m_k}[l_{bce}(D(\boldsymbol{z}_k, \boldsymbol{z}_{-k}, m_k), 1)] + \mathbb{E}_{\boldsymbol{z}_k|m_k, \boldsymbol{z}_{-k}|m_k}[l_{bce}(D(\boldsymbol{z}_k, \boldsymbol{z}_{-k}, m_k), 0)]] \tag{6}$$

5 Experiments

5.1 Experimental Settings

Datasets. We evaluate on one toy dataset and five real-world datasets in various applications, i.e., digit recognition, wearable human activity recognition (WHAR), and machine fault diagnosis. The datasets are described as follows. See Appendix F for more details.

(1) **Toy** dataset is constructed as two-dimensional data with two binary attributes a_1, a_2, as shown in Figure 5a. a_1 has three modes under each attribute value. Data are generated through linearly mapping m_1 and a_2 to two-dimensional spaces and adding noises with noise level σ.

(2) Colored MNIST (**CMNIST**) is constructed from MNIST (LeCun et al., 1998), as shown in Figure 5b. Parity check identifies whether a digit is even or odd with multiple digits under each parity value. Accordingly, a_1 represents parity, m_1 represents the digits, and a_2 represents the color of digits, which is often correlated with digits, e.g., a player's jersey number may be associated with a specific color in sports. Noises are introduced to both digits and colors, and digit noises are generated as occlusions with occlusion ratio as the noise level σ (Chai et al., 2021).

(3) **UCI-HAR** (Anguita et al., 2013), **RealWorld** (Sztyler & Stuckenschmidt, 2016), **HHAR** (Stisen et al., 2015) record wearable sensor data, from which WHAR identifies activities with variations under each activity. Accordingly, a_1 represents activity, m_1 represents unknown activity modes, and a_2 represents user ID, which is often correlated with activity due to personal behavior patterns.

(4) **MFD** (Lessmeier et al., 2016) record sensor data from bearing machines, from which machine fault diagnosis identifies machine fault types with variations under each fault type, e.g., different forms of damages. Accordingly, a_1 represents fault type, m_1 represents unknown modes of fault types, and a_2 represents operating conditions, which could be correlated with machine faults.

Evaluation Protocols. *On toy and CMNIST datasets, correlations are introduced by sampling* (Roth et al., 2023). As illustrated in Figure 6, we train on correlated data and evaluate on 3 test sets, namely test 1 under the same correlations, test 2 without correlations, and test 3 with anticorrelations. The train-test correlation shift increases from test 1 to 3. For comparison with baselines and variants on CMNIST, we train under both attribute correlations and hidden correlations, and report the results on test 3. The complete results on all test sets are in Appendix J. For additional analysis, we train under $cor_h = I(m_1; a_2|a_1) > 0$ to focus on hidden correlations. *On other datasets, we investigate DRL under natural correlations*, where the number of modes and mode labels are unknown. Leave-one-group-out validation is performed, where users and operating conditions in the test group are unseen during training, formulating out-of-distribution (OOD) tasks.

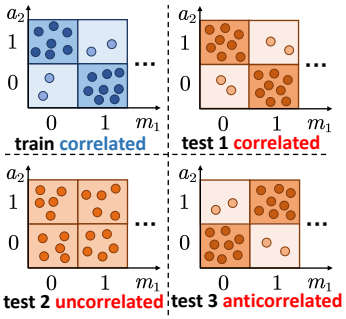

Figure 6: Train-test setup.

On each dataset, we focus on disentangling one attribute with multi-modality as mentioned before. Accuracy (Acc.) and macro F1 score (Mac. F1) are used as performance metrics for attribute prediction. These metrics can reflect the disentanglement of representations under correlation shifts and OOD tasks (Funke et al., 2022; Dittadi et al., 2021), while common disentanglement metrics are not suitable under correlations (Locatello et al., 2020). Each experiment is repeated using 5 varying random seeds, with the mean and standard deviation reported. See details in Appendix F.

Baselines and Implementations. We compare SD-HC with typical DRL methods (**MMD** (Lin et al., 2020), **DTS** (Li et al., 2022), **IDE-VC** (Yuan et al., 2021), and **MI** (Cheng et al., 2022)), and the state-of-the-art DRL methods under correlations (**A-CMI** (Funke et al., 2022) and **HFS** (Oublal et al., 2024)). For reference, we also include the base method trained on supervised prediction losses only, which is denoted as **BASE**, and a variant of our method that uses ground truth mode labels

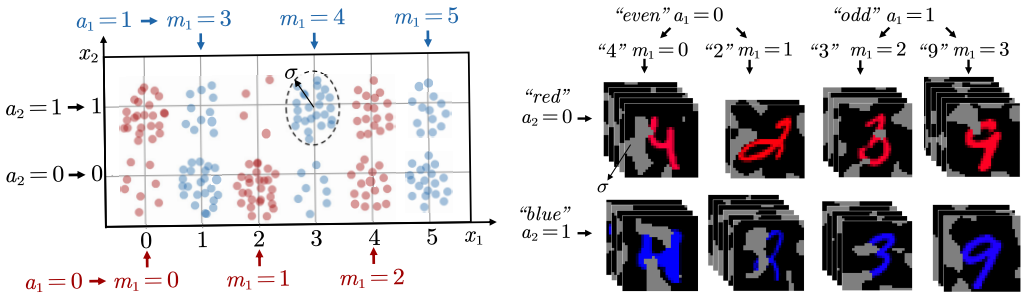

(a) Toy data (b) CMNIST

Figure 5: Data construction of toy dataset and CMNIST with noise level σ.

Table 1: Comparison with baselines (mean±std). "*" indicates that SD-HC is statistically superior to the baselines by pairwise t-test at a 95% significance level. The results of the best methods are **bold**. The results of the runner-up methods are underlined, over which the improvement is calculated.

Method	CMNIST		UCI-HAR		RealWorld		HHAR		MFD	
	Acc.	Mac.	Acc.	Mac. F1	Acc.	Mac. F1	Acc.	Mac. F1	Acc.	Mac. F1
BASE	0.768 ±0.008*	0.768 ±0.008*	0.712 ±0.028*	0.697 ±0.036*	0.646 ±0.014*	0.654 ±0.014*	0.808 ±0.016*	0.809 ±0.020*	0.727 ±0.016*	0.763 ±0.009*
MMD	0.582 ±0.069*	0.528 ±0.117*	0.703 ±0.037*	0.662 ±0.035*	0.660 ±0.019*	0.652 ±0.023*	0.809 ±0.012*	0.805 ±0.017*	0.782 ±0.019*	0.791 ±0.016*
DTS	0.615 ±0.022*	0.615 ±0.022*	0.728 ±0.033*	0.701 ±0.026*	0.644 ±0.023*	0.649 ±0.015*	0.798 ±0.024*	0.797 ±0.017*	0.670 ±0.022*	0.674 ±0.015*
IDE-VC	0.539 ±0.022*	0.533 ±0.027*	0.736 ±0.031*	0.732 ±0.034*	0.652 ±0.013*	0.650 ±0.017*	0.807 ±0.020*	0.806 ±0.014*	0.741 ±0.018*	0.763 ±0.011*
MI	0.611 ±0.039*	0.600 ±0.044*	0.749 ±0.021*	0.745 ±0.027*	0.660 ±0.018*	0.655 ±0.016*	0.809 ±0.017*	0.807 ±0.021*	0.763 ±0.012*	0.776 ±0.016*
A-CMI	0.611 ±0.039*	0.600 ±0.044*	0.714 ±0.034*	0.700 ±0.030*	0.654 ±0.015*	0.655 ±0.012*	0.802 ±0.018*	0.803 ±0.023*	0.788 ±0.014*	0.798 ±0.007*
HFS	0.635 ±0.008*	0.631 ±0.008*	0.671 ±0.035*	0.651 ±0.040*	0.489 ±0.018*	0.398 ±0.015*	0.782 ±0.012*	0.783 ±0.015*	0.754 ±0.017*	0.710 ±0.013*
SD-HC	**0.829** ±0.011	**0.829** ±0.008	**0.830** ±0.03	**0.833** ±0.036	**0.698** ±0.019	**0.699** ±0.014	**0.845** ±0.023	**0.842** ±0.015	**0.825** ±0.020	**0.825** ±0.015
Improvement	↑6.1 %	↑6.1 %	↑7.0 %	↑7.4 %	↑4.0 %	↑4.4 %	↑3.6 %	↑3.5 %	↑3.7 %	↑3.2 %

Table 2: Comparison with variants (mean±std). The notations are the same as Table 1.

Method	CMNIST		UCI-HAR		RealWorld		HHAR		MFD	
	Acc.	Mac. F1	Acc.	Mac. F1	Acc.	Mac. F1	Acc.	Mac. F1	Acc.	Mac. F1
SD-HC-A	0.771 ±0.009*	0.770 ±0.009*	0.822 ±0.023	0.823 ±0.027	0.639 ±0.016*	0.634 ±0.014*	0.819 ±0.016*	0.813 ±0.021	0.815 ±0.016	0.814 ±0.011
SD-HC-MG	0.797 ±0.012*	0.797 ±0.012*	0.822 ±0.020	0.828 ±0.029	0.684 ±0.015*	0.688 ±0.020	0.806 ±0.017*	0.802 ±0.023*	0.803 ±0.015*	0.804 ±0.018*
SD-HC-ID	0.802 ±0.015*	0.802 ±0.15*	0.776 ±0.018	0.768 ±0.023	0.683 ±0.012*	0.678 ±0.011*	0.772 ±0.019*	0.755 ±0.015*	0.806 ±0.017*	0.809 ±0.012
SD-HC-SD	0.783 ±0.010*	0.783 ±0.010*	0.774 ±0.015	0.768 ±0.018	0.662 ±0.013*	0.666 ±0.018*	0.810 ±0.024*	0.812 ±0.018*	0.792 ±0.018*	0.792 ±0.013*
SD-HC-M	0.832 ±0.009*	0.832 ±0.009*	0.796 ±0.029	0.792 ±0.032	0.672 ±0.018*	0.676 ±0.020*	0.839 ±0.023	0.835 ±0.017	0.817 ±0.015	0.817 ±0.020
SD-HC	**0.829** ±0.011	**0.829** ±0.008	**0.830** ±0.03	**0.833** ±0.036	**0.698** ±0.019	**0.699** ±0.014	**0.845** ±0.023	**0.842** ±0.015	**0.825** ±0.020	**0.825** ±0.015

when available, which is denoted as **SD-HC-T**. All methods are implemented using PyTorch (Paszke et al., 2019). Please see Appendix H, F, D, G for details of baselines, implementations, network architectures, and hyper-parameter tuning, respectively. Our codes are available at anonymous Github.

5.2 Comparison with Baseline DRL Methods

The comparison with baseline DRL methods is shown in Table 1, from which we observe:

(1) SD-HC consistently shows superiority over the compared baselines, outperforming the best baseline by an average of 4.86% and 4.92% in accuracy and macro F1 score, respectively. This indicates that SD-HC can better disentangle representations by improving the generalization ability while preserving the predictive ability. For introduced correlations, the large performance gain on CMNIST indicates that SD-HC is advantageous under attribute correlations and strong hidden correlations. For natural correlations, the large performance gain on UCI-HAR indicates the advantage of SD-HC on real-world data with complex multi-modality and hidden correlations.

(2) Despite considering correlations, A-CMI and HFS still fail to improve over BASE in some cases. A-CMI deals with attribute correlations, but fails under hidden correlations in losing mode information. HFS deals with correlations in general, yet its assumption of factorized support might not hold and hurt the predictive ability of representations. For example, in WHAR, HFS assumes that the probability of some user performing some activity could be low, but each user still performs each activity and each activity mode; this is often violated, as users might not perform certain activities due to personalized behavior patterns.

(3) MMD, DTS, IDE-VC, and MI fail to improve over BASE in some cases, because they do not consider correlations and might hurt the predictive ability of representations. Their performance degradation from BASE is especially severe on CMNIST under large train-test correlation shifts.

5.3 Comparison with Variants

We compare with the following variants: **SD-HC-A** additionally minimizes attribute-based CMI for the attributes without multi-modality; **SD-HC-MG** uses Marigold (Mortensen et al., 2023) instead of k-means for clustering in high dimensional spaces; **SD-HC-ID** and **SD-HC-SD** use individual

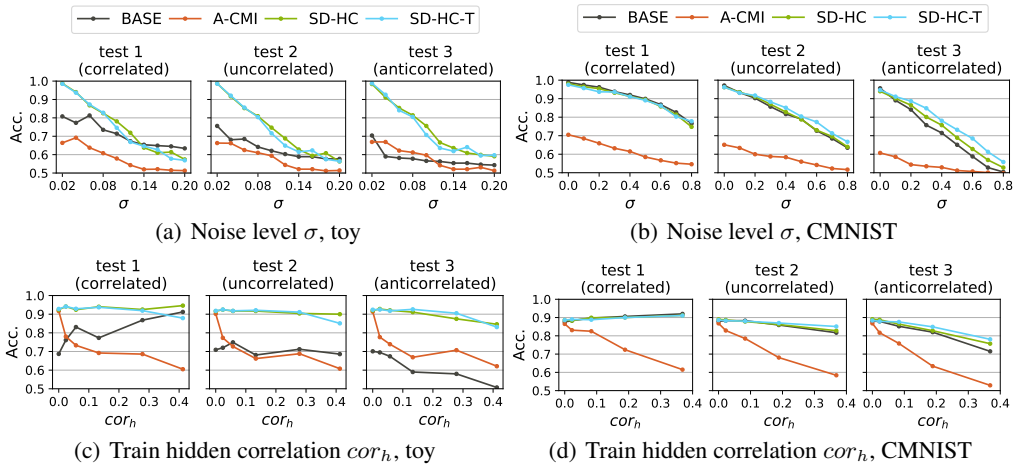

(a) Noise level σ, toy (b) Noise level σ, CMNIST

(c) Train hidden correlation cor_h, toy (d) Train hidden correlation cor_h, CMNIST

Figure 8: Impact of noise level and train hidden correlation on toy and CMNIST datasets.

discriminators and one shared discriminator for different modes, respectively; **SD-HC-M** minimizes mode prediction loss on some inter-mediate representations of encoder. See Appendix D for details.

The results are shown in Table 2, which shows that: (1) SD-HC-A generally does not improve SD-HC, probably because one independence constraint is sufficient for disentanglement, and additional adversarial training objectives might increase training difficulty. (2) SD-HC-MG generally does not improve SD-HC, indicating that k-means is effective for our 128-dimensional representations. Marigold could be considered as an alternative for representations of higher dimensions. (3) SD-HC-ID and SD-HC-SD consistently underperform SD-HC, indicating that proper parameter sharing between different modes in the discriminator is beneficial for mode-based CMI minimization. (4) SD-HC-M consistently underperforms SD-HC, indicating that enforcing mode and attribute prediction on the same representation space benefits the encoding of mode information.

5.4 Method Investigations

Toy Decision Boundary. On toy data, the decision boundaries of the trained predictor of a_1 and the prediction accuracy on the three test sets are shown in Figure 7, from which we observe:

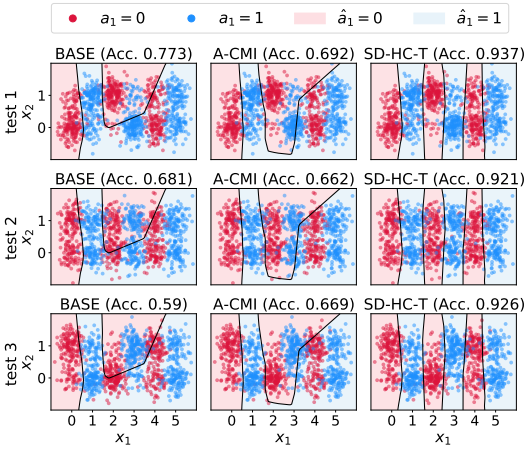

Figure 7: Decision boundary on toy data.

(1) The upper right boundaries of BASE surround the clusters at $a_2 = 1$, and BASE performance decreases as the correlation shift enlarges from test 1 to 3, which indicates that without independence constraints, BASE over-encodes a_2 and lacks generalization ability.

(2) The decision boundaries of A-CMI span across the clusters at $a_2 = 0, 1$ without excluding either value, but fail to separate interleaving clusters at different values of m_1, and the performance is low but robust across 3 test sets, indicating that A-CMI does not over-encode a_2, but loses important mode information.

(3) The decision boundaries of SD-HC-T almost conform to vertical lines $x_1 = b$ that distinguish interleaving clusters, and SD-HC-T shows robustness and superiority across different correlation shifts on 3 test sets. This indicates that SD-HC-T can learn mode information about a_1 (***Informativeness***), and exclude irrelevant information about a_2 (***Independence***), achieving disentanglement.

The Impact of Noise Level and Train Hidden Correlation. The prediction accuracy of a_1 under varying noise levels and train hidden correlations is shown in Figure 8, which shows that:

(1) SD-HC generally shows superiority under varying noises and correlations due to its ability to achieve disentanglement. In addition, the comparable performance of SD-HC and SD-HC-T indicates the effectiveness of mode label estimation by k-means on synthetic and real data.

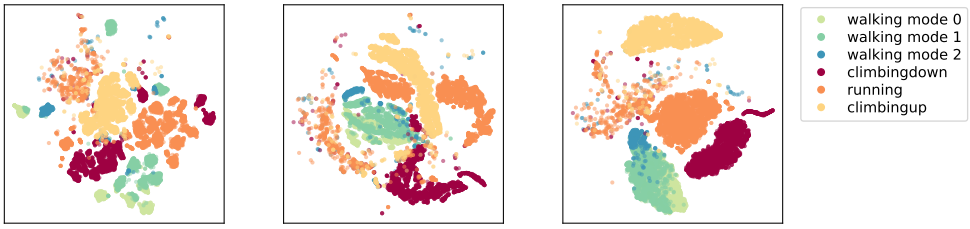

(a) BASE (b) A-CMI (c) SD-HC

Figure 9: Visualization of activity representation distributions on RealWorld. (a), (b), and (c) show the results of four similar activities in BASE, A-CMI, and SD-HC. Compared to SD-HC, activities "walking" and "climbing down" are confused in A-CMI for losing information about walking modes.

(2) In Figure 8a test 1, BASE performs the best at large noise levels, because BASE makes up for the noise-induced information loss by over-encoding a_2. In Figure 8c test 1, BASE performs the best at large train correlations, because when the correlation between m_1 and a_2 is larger, over-encoding a_2 leads BASE to learn more mode information and better predict a_1. As the correlation shift enlarges from test 1 to 3, these advantages are lost due to the lack of generalization ability.

(3) In Figure 8cd, A-CMI performs comparably to SD-HC without hidden correlations ($cor_h = 0$); yet A-CMI performance decreases as hidden correlation increases, because A-CMI does not allow representations to encode shared information induced by hidden correlations, and loses more mode information as hidden correlation increases. The behavior of A-CMI reflects the behavior of common DRL methods that overlook hidden correlations, demonstrating a broader significance.

WHAR Visualizations. On the training set of RealWorld, the data of estimated modes are visualized in Figure 10, which shows that the signals of the three walking modes differ in mean values and volatility, possibly due to varying paces, strides, and postures.

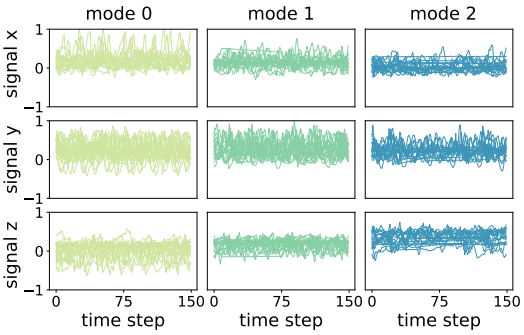

Figure 10: 3-channel accelerometer signals of three walking modes (20 random samples per mode with xyz channels). The x-axis indicates time steps, and the y-axis indicates normalized signals.

The activity representation distributions are visualized by t-SNE in Figure 9, which shows that: (1) **BASE** representations are separated within each activity, probably due to over-encoding user ID and learning personalized user patterns. (2) **A-CMI** representations of different walking modes and different activities are mixed, indicating that different activities are confused due to the loss of mode information. (3) **SD-HC** representations show compactness within each activity, separation between different activities, and partition of different walking modes, indicating independence from user ID and informativeness of activity by encoding mode information.

Additional Analysis. Clustering performance, computational complexity, and parameter sensitivity are analyzed in Appendix I, which show that SD-HC is (1) capable of capturing the underlying modes with k-means clustering, (2) computationally efficient w.r.t. the number of parameters, and (3) not particularly sensitive to changes of N_m when it is slightly above the ground truth value, which is probably because SD-HC can preserve mode information to some extent, as long as the samples within one estimated cluster mostly belong to the same ground-truth mode.

6 Conclusions

In this paper, we propose a novel supervised disentanglement method, SD-HC, that deals with hidden correlations under certain attributes. We introduce mode-based CMI minimization to achieve disentanglement for these certain attributes with multi-modality and hidden correlations, and theoretically prove its sufficiency. Our results can be extended to show the general sufficiency of CMI minimization for disentanglement, demonstrating broad significance. Experiments on the toy dataset and five real-world datasets demonstrate the superiority of SD-HC along with comprehensive investigations.

7 ETHICS STATEMENTS

Our paper mainly focuses on scientific research of supervised disentangled representation learning and there is no potential ethical risk.

8 REPRODUCIBILITY STATEMENTS

We have provided the details regarding computational platforms, dataset descriptions, network architectures, hyper-parameter settings, and the training process of our method in Section 5.1 in the main paper and Appendix D, E, F, and G. Our codes are released at anonymous Github (`https://anonymous.4open.science/r/SD-HC`) as stated in the abstract. The download links of the public datasets are provided in the project homepage and pre-processing functions are included in the codes. The hyper-parameter settings are given in Appendix G.

REFERENCES

Davide Anguita, Alessandro Ghio, Luca Oneto, Xavier Parra Perez, and Jorge Luis Reyes Ortiz. A public domain dataset for human activity recognition using smartphones. In *Proceedings of the International European Symposium on Artificial Neural Networks, Computational Intelligence and Machine Learning*, pp. 437–442, 2013.

Mohamed Ishmael Belghazi, Aristide Baratin, Sai Rajeshwar, Sherjil Ozair, Yoshua Bengio, Aaron Courville, and Devon Hjelm. Mutual information neural estimation. In *Proceedings of the International Conference on Machine Learning*, volume 80, pp. 531–540, 2018.

Diane Bouchacourt, Ryota Tomioka, and Sebastian Nowozin. Multi-level variational autoencoder: Learning disentangled representations from grouped observations. *Proceedings of the AAAI Conference on Artificial Intelligence*, 32(1), 2018.

Malik Boudiaf, Jérôme Rony, Imtiaz Masud Ziko, Eric Granger, Marco Pedersoli, Pablo Piantanida, and Ismail Ben Ayed. A unifying mutual information view of metric learning: Cross-entropy vs. pairwise losses. In *Proceedings of the European Conference on Computer Vision*, pp. 548–564, 2020.

Lucy Chai, Jonas Wulff, and Phillip Isola. Using latent space regression to analyze and leverage compositionality in {gan}s. In *Proceedings of the International Conference on Learning Representations*, 2021.

Junxiang Chen and Kayhan Batmanghelich. Weakly supervised disentanglement by pairwise similarities. *Proceedings of the AAAI Conference on Artificial Intelligence*, 34(04):3495–3502, 2020.

Ling Chen, Rong Hu, Menghan Wu, and Xin Zhou. HMGAN: A hierarchical multi-modal generative adversarial network model for wearable human activity recognition. *Proceedings of the ACM on Interactive, Mobile, Wearable and Ubiquitous Technologies*, 7(3), 2023.

Ricky T. Q. Chen, Xuechen Li, Roger Grosse, and David Duvenaud. Isolating sources of disentanglement in VAEs. *Advances in Neural Information Processing Systems*, pp. 2615–2625, 2018.

Mingyuan Cheng, Xinru Liao, Quan Liu, Bin Ma, Jian Xu, and Bo Zheng. Learning disentangled representations for counterfactual regression via mutual information minimization. In *Proceedings of the International ACM SIGIR Conference on Research and Development in Information Retrieval*, pp. 1802–1806, 2022.

Andrea Dittadi, Frederik Träuble, Francesco Locatello, Manuel Wuthrich, Vaibhav Agrawal, Ole Winther, Stefan Bauer, and Bernhard Schölkopf. On the transfer of disentangled representations in realistic settings. In *Proceedings of the International Conference on Learning Representations*, 2021.

Mhairi Dunion, Trevor McInroe, Kevin Sebastian Luck, Josiah P. Hanna, and Stefano V Albrecht. Conditional mutual information for disentangled representations in reinforcement learning. *Advances in Neural Information Processing Systems*, 2023.

Christina M. Funke, Paul Vicol, Kuan-Chieh Wang, Matthias Kümmerer, Richard Zemel, and Matthias Bethge. Disentanglement and generalization under correlation shifts. In *Proceedings of the Conference on Lifelong Learning Agents*, 2022.

Irina Higgins, Loïc Matthey, Arka Pal, Christopher P. Burgess, Xavier Glorot, Matthew M. Botvinick, Shakir Mohamed, and Alexander Lerchner. Beta-VAE: Learning basic visual concepts with a constrained variational framework. In *Proceedings of the International Conference on Learning Representations*, 2016.

R Devon Hjelm, Alex Fedorov, Samuel Lavoie-Marchildon, Karan Grewal, Phil Bachman, Adam Trischler, and Yoshua Bengio. Learning deep representations by mutual information estimation and maximization. In *Proceedings of the International Conference on Learning Representations*, 2019.

Hyunjik Kim and Andriy Mnih. Disentangling by factorising. In *Proceedings of the International Conference on Machine Learning*, volume 80, pp. 2649–2658, 2018.

Diederik P. Kingma and Jimmy Ba. Adam: A method for stochastic optimization. In *Proceedings of the International Conference on Learning Representations*, 2015.

Yoohwan Kwon, Soo-Whan Chung, and Hong-Goo Kang. Intra-class variation reduction of speaker representation in disentanglement framework. In *Proceedings of Interspeech*, 2020.

Yann LeCun, Léon Bottou, Yoshua Bengio, and Patrick Haffner. Gradient-based learning applied to document recognition. *Proceedings of the IEEE*, 86(11):2278–2324, 1998.

Sang-Hoon Lee, Ji-Hoon Kim, Hyunseung Chung, and Seong-Whan Lee. VoiceMixer: Adversarial voice style mixup. *Advances in Neural Information Processing Systems*, 34:294–308, 2021.

Christian Lessmeier, James Kuria Kimotho, Detmar Zimmer, and Walter Sextro. Condition monitoring of bearing damage in electromechanical drive systems by using motor current signals of electric motors: A benchmark data set for data-driven classification. In *Proceedings of the PHM Society European Conference*, 2016.

Haoliang Li, Sinno Jialin Pan, Shiqi Wang, and Alex C. Kot. Domain generalization with adversarial feature learning. In *Proceedings of the IEEE/CVF Conference on Computer Vision and Pattern Recognition*, pp. 5400–5409, 2018.

Xuelong Li, Mulin Chen, Feiping Nie, and Qi Wang. Locality adaptive discriminant analysis. In *Proceedings of the International Joint Conference on Artificial Intelligence*, pp. 2201–2207, 2017.

Yuening Li, Zhengzhang Chen, Daochen Zha, Mengnan Du, Jingchao Ni, Denghui Zhang, Haifeng Chen, and Xia Hu. Towards learning disentangled representations for time series. In *Proceedings of the SIGKDD Conference on Knowledge Discovery and Data Mining*, pp. 3270–3278, 2022.

Shan Lin, Chang-Tsun Li, and Alex Kot. Multi-domain adversarial feature generalization for person re-identification. *IEEE Transactions on Image Processing*, 30:1596–1607, 2020.

Francesco Locatello, Gabriele Abbati, Tom Rainforth, Stefan Bauer, Bernhard Schölkopf, and Olivier Bachem. On the fairness of disentangled representations. In *Proceedings of the International Conference on Neural Information Processing Systems*, 2019a.

Francesco Locatello, Stefan Bauer, Mario Lucic, Gunnar Raetsch, Sylvain Gelly, Bernhard Schölkopf, and Olivier Bachem. Challenging common assumptions in the unsupervised learning of disentangled representations. In *Proceedings of the International Conference on Machine Learning*, pp. 4114–4124, 2019b.

Francesco Locatello, Stefan Bauer, Mario Lucic, Gunnar Rätsch, Sylvain Gelly, Bernhard Schölkopf, and Olivier Bachem. A sober look at the unsupervised learning of disentangled representations and their evaluation. *Journal of Machine Learning Research*, 21(1), 2020.

Maaten, L. V. D. and Hinton, G. Visualizing data using t-SNE. *Journal of Machine Learning Research*, 9:2579–2605, 2008.

Dhendra Marutho, Sunarna Hendra Handaka, Ekaprana Wijaya, et al. The determination of cluster number at k-mean using elbow method and purity evaluation on headline news. In *2018 international seminar on application for technology of information and communication*, pp. 533–538. IEEE, 2018.

Stefan Matthes, Zhiwei Han, and Hao Shen. Towards a unified framework of contrastive learning for disentangled representations. *Advances in Neural Information Processing Systems*, 2023.

Kasper Overgaard Mortensen, Fatemeh Zardbani, Mohammad Ahsanul Haque, Steinn Ymir Agustsson, Davide Mottin, Philip Hofmann, and Panagiotis Karras. Marigold: Efficient k-means clustering in high dimensions. *Proceedings of the VLDB Endowment*, 16(7):1740–1748, 2023.

Feiping Nie, Zheng Wang, Rong Wang, Zhen Wang, and Xuelong Li. Adaptive local linear discriminant analysis. *ACM Transactions on Knowledge Discovery from Data*, 14(1), 2020.

Khalid Oublal, Said Ladjal, David Benhaiem, Emmanuel LE BORGNE, and François Roueff. Disentangling time series representations via contrastive based l-variational inference. In *Proceedings of the International Conference on Learning Representations*, 2024.

Adam Paszke, Sam Gross, Francisco Massa, Adam Lerer, James Bradbury, Gregory Chanan, Trevor Killeen, Zeming Lin, Natalia Gimelshein, Luca Antiga, et al. Pytorch: An imperative style, high-performance deep learning library. In *Proceedings of the International Conference on Neural Information Processing Systems*, pp. 8026–8037, 2019.

Judea Pearl. Causal diagrams for empirical research. *Biometrika*, 82(4):669–688, 1995.

Judea Pearl. *Causality*. Cambridge University Press, 2 edition, 2009.

Judea Pearl. *Causal inference in statistics: a primer*. John Wiley & Sons, 2016.

Hangwei Qian, Sinno Jialin Pan, and Chunyan Miao. Latent independent excitation for generalizable sensor-based cross-person activity recognition. In *Proceedings of the AAAI Conference on Artificial Intelligence*, volume 35, pp. 11921–11929, 2021.

Mohamed Ragab, Emadeldeen Eldele, Wee Ling Tan, Chuan-Sheng Foo, Zhenghua Chen, Min Wu, Chee-Keong Kwoh, and Xiaoli Li. ADATIME: A benchmarking suite for domain adaptation on time series data. *ACM Transactions on Knowledge Discovery from Data*, 17(8), 2023.

Meitar Ronen, Shahaf E Finder, and Oren Freifeld. DeepDPM: Deep clustering with an unknown number of clusters. In *Proceedings of the IEEE/CVF Conference on Computer Vision and Pattern Recognition*, pp. 9861–9870, 2022.

Karsten Roth, Mark Ibrahim, Zeynep Akata, Pascal Vincent, and Diane Bouchacourt. Disentanglement of correlated factors via hausdorff factorized support. In *Proceedings of the International Conference on Learning Representations*, 2023.

Bernhard Schölkopf, Dominik Janzing, Jonas Peters, Eleni Sgouritsa, Kun Zhang, and Joris Mooij. On causal and anticausal learning. In *Proceedings of the International Conference on Machine Learning*, pp. 459–466, 2012.

Rui Shu, Yining Chen, Abhishek Kumar, Stefano Ermon, and Ben Poole. Weakly supervised disentanglement with guarantees. In *Proceedings of the International Conference on Learning Representations*, 2020.

Peter Spirtes, Clark Glymour, and Richard Scheines. *Causation, prediction, and search*. MIT press, 2001.

Allan Stisen, Henrik Blunck, Sourav Bhattacharya, Thor Siiger Prentow, Mikkel Baun Kjærgaard, Anind Dey, Tobias Sonne, and Mads Møller Jensen. Smart devices are different: Assessing and mitigating mobile sensing heterogeneities for activity recognition. In *Proceedings of the ACM Conference on Embedded Networked Sensor Systems*, pp. 127–140, 2015.

Jie Su, Zhenyu Wen, Tao Lin, and Yu Guan. Learning disentangled behaviour patterns for wearable-based human activity recognition. *Proceedings of the ACM on Interactive, Mobile, Wearable and Ubiquitous Technologies*, 6(1), 2022.

Masashi Sugiyama. Local fisher discriminant analysis for supervised dimensionality reduction. In *Proceedings of the International Conference on Machine Learning*, pp. 905–912, 2021.

Raphael Suter, Djordje Miladinovic, Bernhard Schölkopf, and Stefan Bauer. Robustly disentangled causal mechanisms: Validating deep representations for interventional robustness. In *Proceedings of the International Conference on Machine Learning*, volume 97, pp. 6056–6065, 2019.

Timo Sztyler and Heiner Stuckenschmidt. On-body localization of wearable devices: An investigation of position-aware activity recognition. In *Proceedings of the IEEE International Conference on Pervasive Computing and Communications*, pp. 1–9, 2016.

Frederik Träuble, Elliot Creager, Niki Kilbertus, Anirudh Goyal, Francesco Locatello, Bernhard Schölkopf, and Stefan Bauer. On disentangled representations learned from correlated data. In *Proceedings of the International Conference on Machine Learning*, pp. 10401–10412, 2021.

Yixin Wang and Michael I. Jordan. Desiderata for representation learning: A causal perspective. *arXiv:2109.03795*, 2021.

Sumio Watanabe. A widely applicable bayesian information criterion. *The Journal of Machine Learning Research*, 14(1):867–897, 2013.

Siyang Yuan, Pengyu Cheng, Ruiyi Zhang, Weituo Hao, Zhe Gan, and Lawrence Carin. Improving zero-shot voice style transfer via disentangled representation learning. In *Proceedings of the International Conference on Learning Representations*, 2021.

Junjian Zhang, Chun-Guang Li, Chong You, Xianbiao Qi, Honggang Zhang, Jun Guo, and Zhouchen Lin. Self-supervised convolutional subspace clustering network. In *Proceedings of the IEEE/CVF Conference on Computer Vision and Pattern Recognition*, pp. 5473–5482, 2019.

Roland S. Zimmermann, Yash Sharma, Steffen Schneider, Matthias Bethge, and Wieland Brendel. Contrastive learning inverts the data generating process. In *Proceedings of the International Conference on Machine Learning*, volume 139, pp. 12979–12990, 2021.

A Data Generation Process Under Attribute Correlations

Following (Suter et al., 2019), the data generation process under attribute correlations is formulated in Definition 3. The causal graph of Definition 3 is depicted in Figure 11.

Definition 3. (Disentangled Causal Process). *Consider a causal generative model $p(\boldsymbol{x}|\boldsymbol{a})$ for data $\boldsymbol{x}$ with K attributes $\boldsymbol{a} = (a_1, a_2, ..., a_K)$ as the generative factors, where $\boldsymbol{a}$ could be influenced by L confounders $\boldsymbol{c} = (c_1, ..., c_L)$. This causal model is called disentangled if and only if it can be described by a structural causal model (SCM) (Pearl, 2009) of the form:*

$$\begin{aligned} \boldsymbol{c} &\leftarrow \boldsymbol{n}_c \\ a_i &\leftarrow h_i(S_i^c, \boldsymbol{n}_i), S_i^c \subset \{c_1, ..., c_L\}, i = 1, ..., K \\ \boldsymbol{x} &\leftarrow g(\boldsymbol{a}, \boldsymbol{n}_x) \end{aligned} \tag{7}$$

with functions g, h_i, jointly independent noise variables $\boldsymbol{n}_c$, $\boldsymbol{n}_x$, $\boldsymbol{n}_i$, and confounder subsets S_i^c for $i = 1, ..., K$. Note that $\forall i \neq j, a_i \not\rightarrow a_j$.

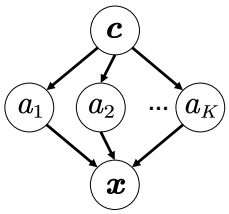

Figure 11: Causal graph of data generation process with attribute correlations.

B Proofs

We give the complete proof of the decomposition and propositions in the main paper using knowledge of mutual information and entropy.

Note that we use formal definitions of mutual information, where separators **semicolon ";"** and **comma ","** should be distinguished from each other. Semicolon ";" separates groups of variables whose mutual information with respect to each other is being measured, while comma "," denotes the joint distribution of the listed variables.

B.1 Proof of Total Hidden Correlation

Total Hidden Correlation $I(m_1; a_2) = I(a_1; a_2) + I(m_1; a_2|a_1)$

Proof. Firstly, we prove $I(m_1; a_2) = I(m_1, a_1; a_2)$. Since each mode falls under one particular attribute value, the value of attribute is fully determined given the modes, i.e., $H(a_1|m_1) = 0$. Therefore, $H(a_1|m_1) = H(a_1|m_1, a_2) + I(a_1; a_2|m_1) = 0$, and followingly $I(a_1; a_2|m_1) = 0$, as both terms are non-negative. Hence $H(a_2|m_1) = H(a_2|m_1, a_1) + I(a_1; a_2|m_1) = H(a_2|m_1, a_1)$. Therefore, we have:

$$\begin{aligned} I(m_1, a_1; a_2) &= H(a_2) - H(a_2|m_1, a_1) \\ &= H(a_2) - H(a_2|m_1) \\ &= I(m_1; a_2) \end{aligned}$$

Secondly, we prove $I(m_1, a_1; a_2) = I(a_1; a_2) + I(m_1; a_2|a_1)$ by chain rule of mutual information:

$$\begin{aligned} I(m_1, a_1; a_2) &= H(a_2) - H(a_2|m_1, a_1) \\ &= H(a_2) - H(a_2|a_1) + H(a_2|a_1) - H(a_2|m_1, a_1) \\ &= I(a_1; a_2) + I(m_1; a_2|a_1) \end{aligned}$$

Finally, we reach $I(m_1; a_2) = I(m_1, a_1; a_2) = I(a_1; a_2) + I(m_1; a_2|a_1)$

B.2 Proof of Proposition 1

Proposition 1. *For representations $\boldsymbol{z}_1, \boldsymbol{z}_2$ of m_1, a_2, respectively, if $I(m_1; a_2|a_1) > 0$, then enforcing $I(\boldsymbol{z}_1; \boldsymbol{z}_2|a_1) = 0$ leads to at least one of $I(\boldsymbol{z}_1; m_1) < H(m_1)$ and $I(\boldsymbol{z}_2; a_2) < H(a_2)$.*

Proof. We prove by contradiction. Assuming $I(\boldsymbol{z}_1; m_1) = H(m_1)$ and $I(a_2; \boldsymbol{z}_2) = H(a_2)$ both stand, we have $H(m_1|\boldsymbol{z}_1) = 0$ and $H(a_2|\boldsymbol{z}_2) = 0$.

Firstly, we prove that this leads to $I(m_1; a_2; \boldsymbol{z}_1; \boldsymbol{z}_2|a_1) > 0$ with (1)(2)(3).

(1) Since $H(m_1|\boldsymbol{z}_1) = 0$ and $H(m_1|\boldsymbol{z}_1) - H(m_1|a_1, \boldsymbol{z}_1) = I(m_1; a_1|\boldsymbol{z}_1) \geq 0$ by definition of conditional mutual information, we have $0 \leq H(m_1|a_1, \boldsymbol{z}_1) \leq H(m_1|\boldsymbol{z}_1) = 0$, we have $H(m_1|a_1, \boldsymbol{z}_1) = 0$. By definition, $H(m_1|a_1, \boldsymbol{z}_1) = H(m_1|a_1, a_2, \boldsymbol{z}_1) + I(m_1; a_2|a_1, \boldsymbol{z}_1) = 0$, which gives $I(m_1; a_2|a_1, \boldsymbol{z}_1) = 0$, as both terms are non-negative. Therefore:

$$\begin{aligned} I(m_1; a_2; \boldsymbol{z}_1|a_1) &= I(m_1; a_2|a_1) - I(m_1; a_2|a_1, \boldsymbol{z}_1) \\ &= I(m_1; a_2|a_1) > 0 \end{aligned}$$

(2) Similar to (1), since $H(a_2|\boldsymbol{z}_2) = 0$ and $0 \leq H(a_2|a_1, \boldsymbol{z}_2) \leq H(a_2|\boldsymbol{z}_2) = 0$, we have $H(a_2|a_1, \boldsymbol{z}_2) = 0$. By definition, $H(a_2|a_1, \boldsymbol{z}_2) = H(a_2|m_1, a_1, \boldsymbol{z}_2) + I(m1; a2|a_1, \boldsymbol{z}_2) = 0$, which gives $I(m_1; a_2|a_1, \boldsymbol{z}_2) = 0$, as both terms are non-negative. Therefore:

$$\begin{aligned} I(m_1; a_2; \boldsymbol{z}_2|a_1) &= I(m_1; a_2|a_1) - I(m_1; a_2|a_1, \boldsymbol{z}_2) \\ &= I(m_1; a_2|a_1) > 0 \end{aligned}$$

(3) Given $H(m_1|\boldsymbol{z}_1) = 0$, we have $H(m_1|\boldsymbol{z}_1) = H(m_1|\boldsymbol{z}_1, \boldsymbol{z}_2) + I(m_1; \boldsymbol{z}_2|\boldsymbol{z}_1) = 0$ and thus $H(m_1|\boldsymbol{z}_1, \boldsymbol{z}_2) = 0$, as both terms are non-negative. Similar to (1) that yields $I(m_1; a_2; \boldsymbol{z}_1|a_1) = I(m_1; a_2|a_1)$ from $H(m_1|\boldsymbol{z}_1) = 0$, we can get $I(m_1; a_2; \boldsymbol{z}_1|a_1, \boldsymbol{z}_2) = I(m_1; a_2|a_1, \boldsymbol{z}_2)$ from $H(m_1|\boldsymbol{z}_1, \boldsymbol{z}_2) = 0$ by additionally conditioning on $\boldsymbol{z}_2$. Combined with $I(m_1; a_2; \boldsymbol{z}_2|a_1) > 0$ in (2), we have:

$$\begin{aligned} I(m_1; a_2; \boldsymbol{z}_1; \boldsymbol{z}_2|a_1) &= I(m_1; a_2; \boldsymbol{z}_1|a_1) - I(m_1; a_2; \boldsymbol{z}_1|a_1, \boldsymbol{z}_2) \\ &= I(m_1; a_2|a_1) - I(m_1; a_2|a_1, \boldsymbol{z}_2) \\ &= I(m_1; a_2; \boldsymbol{z}_2|a_1) > 0 \end{aligned}$$

Secondly, we prove $I(m_1; a_2; \boldsymbol{z}_1; \boldsymbol{z}_2|a_1) \leq 0$ with (4)(5)(6).

(4) Given $H(m_1|a_1, \boldsymbol{z}_1) = 0$ in (1), we have $H(m_1|a_1, \boldsymbol{z}_1) = H(m_1|a_1, \boldsymbol{z}_1, \boldsymbol{z}_2) + I(m_1; \boldsymbol{z}_2|a_1, \boldsymbol{z}_1) = 0$ and followingly, $I(m_1; \boldsymbol{z}_2|a_1, \boldsymbol{z}_1) = 0$, as both terms are non-negative. Therefore:

$$\begin{aligned} I(m_1; \boldsymbol{z}_1; \boldsymbol{z}_2|a_1) &= I(m_1; \boldsymbol{z}_2|a_1) - I(m_1; \boldsymbol{z}_2|a_1, \boldsymbol{z}_1) \\ &= I(m_1; \boldsymbol{z}_2|a_1) \geq 0 \end{aligned}$$

(5) Since $I(\boldsymbol{z}_1; \boldsymbol{z}_2|a_1) = 0$, we have:

$$\begin{aligned} I(m_1; \boldsymbol{z}_1; \boldsymbol{z}_2|a_1) &= I(\boldsymbol{z}_1; \boldsymbol{z}_2|a_1) - I(\boldsymbol{z}_1; \boldsymbol{z}_2|m_1, a_1) \\ &= -I(\boldsymbol{z}_1; \boldsymbol{z}_2|m_1, a_1) \leq 0 \end{aligned}$$

(6) Combine $I(m_1; \boldsymbol{z}_1; \boldsymbol{z}_2|a_1) \geq 0$ in (4) and $I(m_1; \boldsymbol{z}_1; \boldsymbol{z}_2|a_1) \leq 0$ in (5), we have $I(m_1; \boldsymbol{z}_1; \boldsymbol{z}_2|a_1) = 0$. Given $H(m_1|a_1, \boldsymbol{z}_1) = 0$ in (1) and $H(m_1|a_1, \boldsymbol{z}_1) = H(m_1|a_1, \boldsymbol{z}_1, \boldsymbol{z}_2) + I(m_1; \boldsymbol{z}_2|a_1, \boldsymbol{z}_1)$, we have $H(m_1|a_1, \boldsymbol{z}_1, \boldsymbol{z}_2) = 0$ as both terms are non-negative. Similar to (4) that yields $I(m_1; \boldsymbol{z}_1; \boldsymbol{z}_2|a_1) = I(m_1; \boldsymbol{z}_2|a_1)$ from $H(m_1|a_1, \boldsymbol{z}_1) = 0$, we can get $I(m_1; \boldsymbol{z}_1; \boldsymbol{z}_2|a_1, a_2) = I(m_1; \boldsymbol{z}_2|a_1, a_2)$ from $H(m_1|a_1, \boldsymbol{z}_1, \boldsymbol{z}_2) = 0$ by additionally conditioning on $\boldsymbol{z}_2$. Therefore:

$$\begin{aligned} I(m_1; a_2; \boldsymbol{z}_1; \boldsymbol{z}_2|a_1) &= I(m_1; \boldsymbol{z}_1; \boldsymbol{z}_2|a_1) - I(m_1; \boldsymbol{z}_1; \boldsymbol{z}_2|a_1, a_2) \\ &= -I(m_1; \boldsymbol{z}_2|a_1, a_2) \leq 0 \end{aligned}$$

This is contradictory with $I(m_1; a_2; \boldsymbol{z}_1; \boldsymbol{z}_2|a_1) > 0$. Therefore, if $I(m_1; a_2|a_1) > 0$ and $I(\boldsymbol{z}_1; \boldsymbol{z}_2|a_1) = 0$, then at least one of $I(m_1; \boldsymbol{z}_1) < H(m_1)$ and $I(a_2; \boldsymbol{z}_2) < H(a_2)$ must hold.

B.3 Proof of Proposition 2

Proposition 2. *For representations $\boldsymbol{z}_1, \boldsymbol{z}_2$ of m_1, a_2, respectively, if $I(\boldsymbol{z}_1; m_1) = H(m_1)$, $I(\boldsymbol{z}_2; a_2) = H(a_2)$, and $I(\boldsymbol{z}_1; \boldsymbol{z}_2|m_1) = 0$, then $I(\boldsymbol{z}_1; a_2) = I(m_1; a_2)$ and $I(\boldsymbol{z}_1; a_2|m_1) = 0$.*

Proof. First, we prove $I(m_1; a_2) \geq I(\boldsymbol{z}_1; \boldsymbol{z}_2)$ with (1)(2).

(1) Since $H(a_2|\boldsymbol{z}_2) = 0$, we have $H(a_2|\boldsymbol{z}_2) = H(a_2|\boldsymbol{z}_1, \boldsymbol{z}_2) + I(\boldsymbol{z}_1; a_2|\boldsymbol{z}_2) = 0$, and followingly $I(\boldsymbol{z}_1; a_2|\boldsymbol{z}_2) = 0$, as both terms are non-negative. Therefore, by definition of interaction information,

we have $I(\boldsymbol{z}_1;\boldsymbol{z}_2;a_2) = I(\boldsymbol{z}_1;a_2) - I(\boldsymbol{z}_1;a_2|\boldsymbol{z}_2) = I(\boldsymbol{z}_1;a_2)$. Since $I(\boldsymbol{z}_1;\boldsymbol{z}_2|m_1) = 0$, we have $I(\boldsymbol{z}_1;\boldsymbol{z}_2;a_2|m_1) = I(\boldsymbol{z}_1;\boldsymbol{z}_2|m_1) - I(\boldsymbol{z}_1;\boldsymbol{z}_2|m_1,a_2) = -I(\boldsymbol{z}_1;\boldsymbol{z}_2|m_1,a_2)$. Therefore:

$$\begin{aligned} I(\boldsymbol{z}_1;\boldsymbol{z}_2;m_1;a_2) &= I(\boldsymbol{z}_1;\boldsymbol{z}_2;a_2) - I(\boldsymbol{z}_1;\boldsymbol{z}_2;a_2|m_1) \\ &= I(\boldsymbol{z}_1;a_2) + I(\boldsymbol{z}_1;\boldsymbol{z}_2|m_1,a_2) \\ &\geq I(\boldsymbol{z}_1;a_2) \end{aligned}$$

(2) i. Since $H(a_2|\boldsymbol{z}_2) = 0$, we have $H(a_2|\boldsymbol{z}_2) = H(a_2|m_1,\boldsymbol{z}_2) + I(m_1;a_2|\boldsymbol{z}_2) = 0$, and followingly $I(m_1;a_2|\boldsymbol{z}_2) = 0$, as both terms are non-negative.

ii. Since $H(m_1|\boldsymbol{z}_1) = 0$, we have $H(m_1|\boldsymbol{z}_1) = H(m_1|\boldsymbol{z}_1,\boldsymbol{z}_2) + I(m_1;\boldsymbol{z}_2|\boldsymbol{z}_1) = 0$, and followingly $H(m_1|\boldsymbol{z}_1,\boldsymbol{z}_2) = 0$, as both terms are non-negative. Therefore, $H(m_1|\boldsymbol{z}_1,\boldsymbol{z}_2) = H(m_1|\boldsymbol{z}_1,\boldsymbol{z}_2,a_2) + I(m_1;a_2|\boldsymbol{z}_1,\boldsymbol{z}_2) = 0$, and followingly $I(m_1;a_2|\boldsymbol{z}_1,\boldsymbol{z}_2) = 0$, as both terms are non-negative.

iii. Given $I(m_1;a_2|\boldsymbol{z}_2) = 0$ in i. and $I(m_1;a_2|\boldsymbol{z}_1,\boldsymbol{z}_2) = 0$ in ii. as shown above, we have $I(m_1;a_2;\boldsymbol{z}_1|\boldsymbol{z}_2) = I(m_1;a_2|\boldsymbol{z}_2) - I(m_1;a_2|\boldsymbol{z}_1,\boldsymbol{z}_2) = 0$.

iv. Since $H(m_1|\boldsymbol{z}_1) = 0$, by definition of conditional mutual information, we have $H(m_1|\boldsymbol{z}_1) = H(m_1|\boldsymbol{z}_1,a_2) + I(m_1;a_2|\boldsymbol{z}_1) = 0$, and followingly $I(m_1;a_2|\boldsymbol{z}_1) = 0$, as both terms are non-negative. Thus $I(m_1;a_2;\boldsymbol{z}_1) = I(m_1;a_2) - I(m_1;a_2|\boldsymbol{z}_1) = I(m_1;a_2)$.

Given $I(m_1;a_2;\boldsymbol{z}_1) = I(m_1;a_2)$ in iv. and $I(m_1;a_2;\boldsymbol{z}_1|\boldsymbol{z}_2) = 0$ in iii., we have:

$$\begin{aligned} I(\boldsymbol{z}_1;\boldsymbol{z}_2;m_1;a_2) &= I(m_1;a_2;\boldsymbol{z}_1) - I(m_1;a_2;\boldsymbol{z}_1|\boldsymbol{z}_2) \\ &= I(m_1;a_2) \end{aligned}$$

Given (1)(2), we have $I(m_1;a_2) = I(\boldsymbol{z}_1;\boldsymbol{z}_2;m_1;a_2) \geq I(\boldsymbol{z}_1;a_2)$

(3) We prove $I(\boldsymbol{z}_1;a_2) \geq I(m_1;a_2)$ as follows.

i. Since $H(m_1|\boldsymbol{z}_1) = 0$, we have $H(m_1|\boldsymbol{z}_1) = H(m_1|\boldsymbol{z}_1,a_2) + I(m_1;a_2|\boldsymbol{z}_1) = 0$, and followingly $I(m_1;a_2|\boldsymbol{z}_1) = 0$, as both terms are non-negative. Thus, by chain rule of mutual information, we have:

$$\begin{aligned} I(m_1,\boldsymbol{z}_1;a_2) &= I(\boldsymbol{z}_1;a_2) + I(m_1;a_2|\boldsymbol{z}_1) \\ &= I(\boldsymbol{z}_1;a_2) \end{aligned}$$

ii. We also have:

$$\begin{aligned} I(m_1,\boldsymbol{z}_1;a_2) &= I(m_1;a_2) + I(\boldsymbol{z}_1;a_2|m_1) \\ &\geq I(m_1;a_2) \end{aligned}$$

Given $I(m_1,\boldsymbol{z}_1;a_2) = I(\boldsymbol{z}_1;a_2)$ in i. and , $I(m_1,\boldsymbol{z}_1;a_2) \geq I(m_1;a_2)$ in ii., we have $I(\boldsymbol{z}_1;a_2) \geq I(m_1;a_2)$.

(4) Finally, given $I(m_1;a_2) \geq I(\boldsymbol{z}_1;a_2)$ with (1)(2) and $I(\boldsymbol{z}_1;a_2) \geq I(m_1;a_2)$ in (3), the equality must hold that $I(\boldsymbol{z}_1;a_2) = I(m_1;a_2)$.

Moving forward, given $I(m_1,\boldsymbol{z}_1;a_2) = I(\boldsymbol{z}_1;a_2) = I(m_1;a_2) + I(\boldsymbol{z}_1;a_2|m_1)$ in (3) and $I(\boldsymbol{z}_1;a_2) = I(m_1;a_2)$ at which we just arrived, we have $I(\boldsymbol{z}_1;a_2|m_1) = 0$.

B.4 Proof of Proposition 3

Proposition 3. *Under the data generation assumption of Definition 1 ($K = 2$, $k = 1$) with independent mechanisms, if $I(\boldsymbol{z}_1;a_2|m_1) = 0$ for representation $\boldsymbol{z}_1$, then $p(\boldsymbol{z}_1|\mathrm{do}(a_2)) = p(\boldsymbol{z}_1)$.*

Proof. We prove this by applying Rule 3 of do-calculus based on the causal graph G in Figure 12. The rules of do-calculous are elaborated in Appendix C.1, where $\perp\!\!\!\perp$ indicates independence between variables. Specifically, we unfold the left-hand side of $p(\boldsymbol{z}_1|\mathrm{do}(a_2)) = p(\boldsymbol{z}_1)$ and reach the

right-hand side as:

$$p(\boldsymbol{z}_1|\text{do}(a_2)) = \sum_{m_1} p(\boldsymbol{z}_1|\text{do}(a_2), m_1)p(m_1|\text{do}(a_2)) \quad \text{(i)}$$
$$= \sum_{m_1} p(\boldsymbol{z}_1|m_1)p(m_1) \quad \text{(ii)}$$
$$= p(\boldsymbol{z}_1) \quad \text{(iii)}$$

where we arrive at (i) by chain rule of probability, and then arrive at (ii) by using Rule 3 of do-calculus twice: First, given $I(\boldsymbol{z}_1; a_2|m_1) = 0$, we have $\boldsymbol{z}_1 \perp\!\!\!\perp a_2|m_1$ in G, as the mutual information between variables equals zero if and only if they are independent; Since this conditional independence about $\boldsymbol{z}_1$ is determined by the representation learning with the parameterized encoder rather than the data generation process, removing edges from confounders to a_2 should not impact the conditional independence about $\boldsymbol{z}_1$ according to causal sufficiency (Spirtes et al., 2001), i.e., $\boldsymbol{z}_1 \perp\!\!\!\perp a_2|m_1$ also holds in $G_{\overline{a_2(m_1)}} = G_{\overline{a_2}}$, where the notations are defined in Appendix C.1; now we satisfy the condition of Rule 3 and apply do-calculous as:

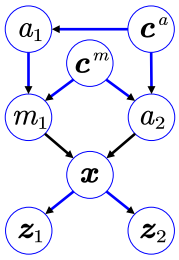

Figure 12: Causal graph of representation learning.

$p(\boldsymbol{z}_1|\text{do}(a_2), m_1) = p(\boldsymbol{z}_1|m_1)$ Rule 3 by $\boldsymbol{z}_1 \perp\!\!\!\perp a_2|m_1$ in $G_{\overline{a_2}}$ (representation learning)

Second, given the causal independence assumption between attributes in Definition 1, we satisfy the condition of Rule 3 and apply do-calculous as:

$p(m_1|\text{do}(a_2)) = p(m_1)$ Rule 3 by $m_1 \perp\!\!\!\perp a_2$ in $G_{\overline{a_2}}$ (independent mechanisms)

Finally, we arrive at (iii) by chain rule of probability.

Discussions. Our proof mainly relies on two conditions: (1) the causal independence between m_1 and a_2, which comes from the *independent mechanism assumption* (Schölkopf et al., 2012) of data, and (2) conditional independence $I(\boldsymbol{z}_1; a_2|m_1) = 0$, which is enforced upon $\boldsymbol{z}_1$ by representation learning that minimizes mode-based CMI, as proved in Proposition 2. Thereby, we conclude that *for data generated by independent mechanisms, disentangled representations can be learned by mode-based CMI minimization and supervised learning*.

B.5 Generalization of Theoretical Results

Our theoretical results, including the necessary condition and the sufficient condition for disentanglement, can be generalized to multiple attributes. The extension mainly involves replacing $m_1, \boldsymbol{z}_1$ with $m_k, \boldsymbol{z}_k$, and replacing $a_2, \boldsymbol{z}_2$ with the joint $a_{-k}, \boldsymbol{z}_{-k}$, as the properties of mutual information and causal graphs remain the same for joint variables.

Specifically, the necessary condition in Figure 3 is extended to K attributes in Figure 13, where the necessary condition for disentanglement under hidden correlations and potential attribute correlations is $I(\boldsymbol{z}_k; \boldsymbol{z}_{-k}|m_k) = 0$.

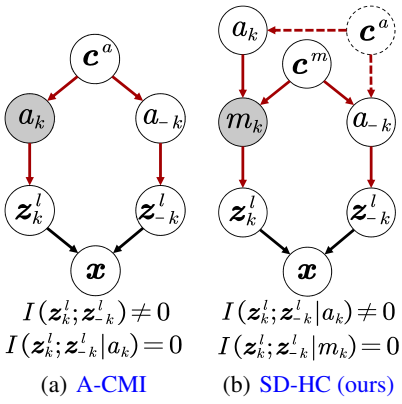

Figure 13: Causal graphs of the true latent representations under $K > 2$. **Red** arrows indicate the *backdoor paths* between $\boldsymbol{z}_1^l$ and $\boldsymbol{z}_2^l$. The dashed circle and arrows indicate that attribute correlations may or may not exist.

For the sufficient condition of disentanglement, we extend Proposition 2 to Corollary 2.1 for $K > 2$. The constraint $I(a_k; \boldsymbol{z}_k) = H(a_k)$ is added, yet this is implied in $I(\boldsymbol{z}_k; m_k) = H(m_k)$, because each mode falls under only one attribute value, and the value of the attribute is determined knowing the mode. In other words, the information contained in a_k is already contained in m_k. In addition, the joint constraint $I(\boldsymbol{z}_{-k}; a_{-k}) = H(a_{-k})$ is broken down for each $i \neq k$, i.e., $I(\boldsymbol{z}_i; a_i) = H(a_i), i \neq k$.

Corollary 2.1 *For representations $\boldsymbol{z}_i$ of a_i ($i = 1, ..., K$), if $I(\boldsymbol{z}_i; a_i) = H(a_i)$ for $i = 1, ..., K$, $I(\boldsymbol{z}_k; m_k) = H(m_k)$, and $I(\boldsymbol{z}_k; \boldsymbol{z}_{-k}|m_k) = 0$ for a specific $1 < k < K$, then $I(\boldsymbol{z}_k; a_{-k}) = I(m_k; a_{-k})$ and $I(\boldsymbol{z}_k; a_{-k}|m_k) = 0$.*

where $-k$ indicates the set of attribute indices $\{j\}_{j \neq k}$.

In addition, we extend Proposition 3 to Corollary 3.1 for $K > 2$ as follows.

Corollary 3.1. *Under the data generation assumption of Definition 1 with independent mechanisms, if $I(\boldsymbol{z}_k; a_{-k}|m_k) = 0$ for representation $\boldsymbol{z}_k$, then $p(\boldsymbol{z}_k|\mathrm{do}(a_{-k})) = p(\boldsymbol{z}_k)$.*

C CAUSALITY

C.1 D-SEPARATION AND BACKDOOR PATHS

Overview of Causality We provide a summary of notions in causal graphs relevant to the analysis in Section 3.3, namely d-separation, blocking paths, and conditional independence. More details can be found in (Pearl, 2009).

Causal graphs are directed acyclic graphs, where nodes represent random variables and directed edges represent the causal relationships between two variables. The notion of d-separation forms the link between blocking paths in the causal graph and dependencies between random variables. A *path* in causal graphs is a sequence of consecutive edges. Consider two nodes X and Y, X and Y are called *d-separated* by a set of nodes Z if all undirected paths from X to Y are *blocked* by Z. Meanwhile, a path between X and Y is considered to be *blocked* by a set of nodes Z if at least one of the following holds:

(1) The path contains a chain $X \to M \to Y$ with the mediator set M, and a node in M is in Z.

(2) The path contains a fork $X \leftarrow U \to Y$ with the confounder set U, and a node in U is in Z.

(3) The path contains a collider $X \to C \leftarrow Y$ with the collider node C, and neither C or its descendant is in Z.

Finally, if X and Y are d-separated by the set Z, X and Y are conditionally independent given Z. A *backdoor path* between X and Y is the non-causal path between X and Y that contains at least one edge pointing at X or Y, i.e. the path that flows backward from X or Y. Backdoor paths introduce dependence between variables, thus they need to be blocked by controlling a node on these paths as in (1) and (2).

Causal Graph Analysis Under Hidden Correlations Figure 3b contains three paths between $\boldsymbol{z}_1$ and $\boldsymbol{z}_2$. (1) The path $\boldsymbol{z}_1 \to \boldsymbol{x} \leftarrow \boldsymbol{z}_2$ is blocked without conditioning on any variables, as long as the collider $\boldsymbol{x}$ is uncontrolled. (2) The path $\boldsymbol{z}_1 \leftarrow m_1 \leftarrow \boldsymbol{c}^m \to a_2 \to \boldsymbol{z}_2$ is blocked if any node in the confounder set $\{m_1, \boldsymbol{c}^m, a_2\}$ is controlled. Since $\boldsymbol{c}^m$ is unobserved, controlling either m_1 or a_2 blocks this path. (3) The path $\boldsymbol{z}_1 \leftarrow m_1 \leftarrow a_1 \leftarrow \boldsymbol{c}^a \to a_2 \to \boldsymbol{z}_2$ is blocked if any node in the confounder set $\{m_1, a_1, \boldsymbol{c}^a, a_2\}$ is controlled. Since $\boldsymbol{c}^a$ is unobserved, controlling one of m_1, a_1, and a_2 blocks this path. To simultaneously block all undirected paths between $\boldsymbol{z}_1$ and $\boldsymbol{z}_2$, we need to control either m_1 or a_2, as controlling a_1 does not block path (2). That is to say, $\boldsymbol{z}_1$ and $\boldsymbol{z}_2$ are conditionally independent given either m_1 or a_2.

C.2 RULES OF *do*-CALCULUS

Let X, Y, Z, and W be arbitrary disjoint sets of nodes in a causal DAG G. *do*-calculus consists of three inference rules that permit us to map interventional and observational distributions to each other whenever certain conditions hold in the causal diagram G.

We denote by $G_{\overline{X}}$ the graph obtained by deleting from G all arrows pointing to nodes in X. Likewise, we denote by $G_{\underline{X}}$ the graph obtained by deleting from G all arrows emerging from nodes in X. To represent the deletion of both incoming and outgoing arrows, we use the notation $G_{\overline{X}\underline{Z}}$. The following three rules are valid for every interventional distribution compatible with G (Pearl, 2016; 1995).

- ***Rule 1**: Insertion/deletion of observations*

$$P(y|do(x), z, w) = P(y|do(x), w), \quad \text{if } Y \perp\!\!\!\perp Z|X, W \text{ in } G_{\overline{X}}$$

Table 3: Network architectures. "Discriminator(a_{in})" denotes discriminator with conditional input a_{in}. "Conv(ci, kj, sl)" denotes 1D convolution layer with i channels, kernel size j, and stride l. "FC(i)" denotes fully connected layer with output dimension i. "BN(i)" denotes 1D batch normalization layer with feature dimension i. "AvgPool(i)" denotes 1D adaptive pooling layer with output dimension i. "LeakyReLU(α)" denotes LeakyReLU activations with scale α. Output dimension d_{out} is set according to each prediction task. N_1^c and N_2^c denote the number of values for a_1 and a_2, respectively.

Component	Method	Dataset	Architectures
Encoder subnetwork	All	Toy	FC(16) → FC(16)
Encoder subnetwork	All	CMNIST	FC(128), BN(128) → FC(128), BN(128)
Encoder subnetwork	All	WHAR	Conv(c128, k8, s2), BN(128) → Conv(c256, k5, s2), BN(256) → Conv(c128, k3, s1), BN(128), AvgPool(1)
Encoder subnetwork	All	MFD	Conv(c64, k32, s6), BN(64) → Conv(c128, k8, s2), BN(128) → Conv(c128, k8, s2), BN(128), AvgPool(1)
Predictor	All	All	FC(d_{out}), Softmax
Discriminator(m_1)	SD-HC	All	N_1^c × [FC(512), LeakyReLu(0.2) → FC(1), Sigmoid] for each value of a_1
Discriminator(-)	SD-HC-A	All	N_2^c × [FC(512), LeakyReLu(0.2) → FC(1), Sigmoid] for each value of a_2
Discriminator(-)	SD-HC-ID	All	N_1^c × N_m× [FC(512), LeakyReLu(0.2) → FC(1), Sigmoid] for each mode under each value of a_1
Discriminator(a_1, m_1)	SD-HC-SD	All	FC(512), LeakyReLu(0.2) → FC(1), Sigmoid
Middle layer	SD-HC-M	All	FC(128), BN(128)

- ***Rule 2**: Action/observation exchange*

$$P(y|do(x), do(z), w) = P(y|do(x), z, w), \quad \text{if } Y \perp\!\!\!\perp Z|X, W \text{ in } G_{\overline{X}\underline{Z}}$$

- ***Rule 3**: Insertion/deletion of actions*

$$P(y|do(x), do(z), w) = P(y|do(x), w), \quad \text{if } Y \perp\!\!\!\perp Z|X, W \text{ in } G_{\overline{XZ(W)}}$$

where $\perp\!\!\!\perp$ indicates independence, and $Z(W)$ is the set of Z-nodes that are not ancestors of any W-node in $G_{\overline{X}}$.

D Network Architectures

The detailed architectures of different components in SD-HC and its variants are summarized in Table 3. For independent control of each attribute, encoder F uses individual subnetworks for each attribute with the same architectures. Predictors C_i, C_i^m share the same architectures as well. Different architectures of discriminator D_k in SD-HC, SD-HC-A, SD-HC-ID, and SD-HC-SD, and the architecture of the middle layer in SD-HC-M are described separately. SD-HC-M calculates the mode prediction loss on the output representations $\boldsymbol{z}_k$ of encoder F with C_k^m, passes $\boldsymbol{z}_k$ to the middle layer, and calculates the attribute prediction loss on the output representations of the middle layer with C_k.

E Training Process

The training process of SD-HC under $K = 2$ (a_1 as the attribute with multi-modality) is summarized in Algorithm 1, where optimizations w.r.t. different losses are performed alternatively. The algorithm can be generalized to multiple attributes accordingly.

F Details of Experimental Settings

F.1 Datasets

Toy Dataset Our 2-dimensional toy data have two binary attributes, with the primary attribute a_1 having 3 modes under each attribute value, i.e., $a_1 = 0, m_1 = 0, 1, 2$ and $a_1 = 1, m_1 = 3, 4, 5$. Data are generated from the attributes as $\boldsymbol{x} = \boldsymbol{m}_1 \cdot [[0, 0], [2, 0], [4, 0], [1, 0], [3, 0], [5, 0]] + \boldsymbol{a}_2 \cdot$

Algorithm 1 The training process of SD-HC under $K = 2$

Input: Training set $\mathcal{D}$ with data $\boldsymbol{x}$ and attributes labels $\boldsymbol{a} = (a_1, a_2)$, the number of modes N_m under each value of a_1, the number of epochs E_1 and E_2, and the number of steps S_{d}, S_{f}, and S_{c}
Initialize encoder F^* and predictor C_1^*
for $epoch = 1$ **to** E_1 **do**
  for mini-batch $(\boldsymbol{x}, a_1)$ **in** $\mathcal{D}$ **do**
    Update F^* and C_1^* by minimizing $\mathcal{L}_{ac}$ in Equation 4
  end for
end for
Under each value of a_1, perform k-means clustering with the number of clusters N_m on the output representations $\boldsymbol{z}_1$ of the trained encoder F^*, and get the estimated mode labels m_1
Initialize encoder F, predictors C_1, C_2, C_1^m, and discriminator D_1
for $epoch = 1$ **to** E_2 **do**
  for mini-batch $(\boldsymbol{x}, \boldsymbol{a})$ **in** $\mathcal{D}$ **do**
    for $step = 1$ **to** S_{c} **do**
      Update encoder F and predictors C_1, C_2 and C_1^m by minimizing $\mathcal{L}_c$ in Equation 5
    end for
    for $step = 1$ **to** S_{d} **do**
      Update discriminator D_1 by minimizing $\mathcal{L}_d$ in Equation 6
    end for
    for $step = 1$ **to** S_{f} **do**
      Update encoder F by maximizing $\mathcal{L}_d$ in Equation 6
    end for
  end for
end for
Output: Encoder F and predictor C_1

Table 4: Dataset descriptions.

Dataset	UCI-HAR	RealWorld	HHAR	MFD
a_1	activity	activity	activity	incipient fault type
a_2	user	user	user	operating condition
# values of a_1	6	8	6	3
# values of a_2	30	15	9	4
# of groups	5	5	3	4
# channels	3	3	3	1
# samples	11711	36980	14772	10916
window length	128	150	128	5120
values of a_1	walking, walking upstairs, walking downstairs, sitting, standing, laying	climbing stairs up, climbing stairs down, jumping, lying, standing, sitting, running, walking	healthy, inner-bearing damage, outer-bearing damage	

$[[0, 0], [0, 1]] + \boldsymbol{n}$, where vectors $\boldsymbol{m}_1$ and $\boldsymbol{a}_2$ represent the one-hot encoded values of m_1 and a_2, respectively, and $\boldsymbol{n} \sim \mathcal{N}(\boldsymbol{0}, \sigma^2 \boldsymbol{I})$ represents 2-dimensional independently normally distributed noise with noise level σ. For $\boldsymbol{x} = (x_1, x_2)$, the primary attribute a_1 and mode m_1 control dimension 1, i.e., x_1, and attribute a_2 controls dimension 2, i.e., x_2. An illustration of the generated data under different correlations and noise levels is given in Figure 14.

Table 5: Conditional probability $p(a_2|m_1)$ on toy data for $cor_h = 0$.

$p(a_2\|m_1)$		m_1					
		0	1	2	3	4	5
a_2	0	0.5	0.5	0.5	0.5	0.5	0.5
	1	0.5	0.5	0.5	0.5	0.5	0.5

Table 6: Conditional probability $p(a_2|m_1)$ on toy data for $cor_h = 0.02$.

$p(a_2\|m_1)$		m_1					
		0	1	2	3	4	5
a_2	0	0.6	0.3	0.6	0.5	0.6	0.4
	1	0.4	0.7	0.4	0.5	0.4	0.6

Table 7: Conditional probability $p(a_2|m_1)$ on toy data for $cor_h = 0.06$.

$p(a_2\|m_1)$		m_1					
		0	1	2	3	4	5
a_2	0	0.7	0.2	0.6	0.4	0.7	0.4
	1	0.3	0.8	0.4	0.6	0.3	0.6

Table 8: Conditional probability $p(a_2|m_1)$ on toy data for $cor_h = 0.13$.

$p(a_2\|m_1)$		m_1					
		0	1	2	3	4	5
a_2	0	0.8	0.1	0.6	0.3	0.8	0.4
	1	0.2	0.9	0.4	0.7	0.2	0.6

Table 9: Conditional probability $p(a_2|m_1)$ on toy data for $cor_h = 0.28$.

$p(a_2\|m_1)$		m_1					
		0	1	2	3	4	5
a_2	0	0.9	0	0.6	0.2	0.9	0.4
	1	0.1	1	0.4	0.8	0.1	0.6

Table 10: Conditional probability $p(a_2|m_1)$ on toy data for $cor_h = 0.41$.

$p(a_2\|m_1)$		m_1					
		0	1	2	3	4	5
a_2	0	1	0	0.5	0.1	1	0.4
	1	0	1	0.5	0.9	0	0.6

Table 11: Conditional probability $p(a_2|m_1)$ on CMNIST under attribute correlations and hidden correlations.

$p(a_2\|m_1)$		m_1			
		0	1	2	3
a_2	0	0.8	0.05	0.2	0.95
	1	0.2	0.95	0.8	0.05

Table 12: Conditional probability $p(a_2|m_1)$ on CMNIST under only hidden correlations.

$p(a_2\|m_1)$		m_1			
		0	1	2	3
a_2	0	$corr_p$	$1 - corr_p$	$corr_p$	$1 - corr_p$
	1	$1 - corr_p$	$corr_p$	$1 - corr_p$	$corr_p$

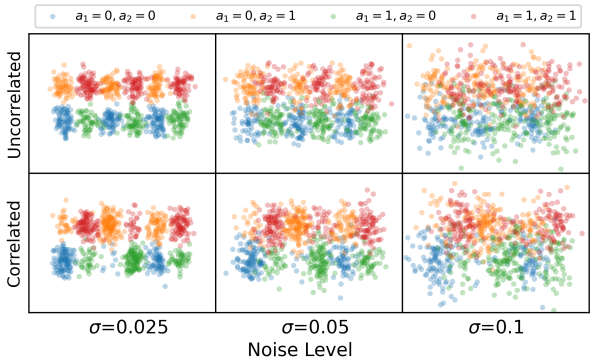

Figure 14: Generated toy data under different correlations and noise levels.

CMINIST Dataset Colored MNIST (**CMNIST**) is constructed by coloring and occluding a subset of MNIST (LeCun et al., 1998). As shown in Figure 5b, attribute a_1 is defined as the parity of digits, i.e., $a_1 = 0, 1$ indicates "even", "odd". Attribute a_2 is defined as the color of digits, i.e., $a_2 = 0, 1$ indicates "red", "blue". a_1 has 2 modes under each attribute value, i.e., digits 4, 2 under parity "even" and digits 3, 9 under parity "odd". Digit noises are generated as occlusion masks with occlusion ratio as the noise level σ (Chai et al., 2021), and coloring noises are generated as a scalar multiplier to the RGB values of the digits.

Time Series Datasets We use acceleration signals from UCI-HAR, RealWorld, and HHAR datasets and vibration signals from MFD dataset. After removing invalid values and normalizing the data by channel to be within the range of [-1, 1], we pre-process the data by the sliding window strategy. For WHAR datasets with multiple sensors, we use the 3-axis acceleration data from the waist for UCI-HAR, the acceleration data from the chest for RealWorld, and the acceleration data from a Samsung smartphone for HHAR following (Ragab et al., 2023). Table 4 summarizes the statistics of the preprocessed data used in our experiments.

F.2 Evaluation Protocol

Toy Since we focus on investigating the behavior of different methods under only hidden correlations $I(m_1; a_2|a_1) > 0$, data are set to be uniformly distributed under the values of m_1, a_1, and a_2, and attribute correlations do not exist, i.e., $I(a_1; a_2) = 0$. The hidden correlations are introduced by setting $p(a_2|m_1)$ to Table 5, 6, 7, 8, 9, 10 for hidden correlations $cor_h = 0, 0.02, 0.06, 0.13, 0.28, 0.41$, respectively.

CMNIST Since we focus on investigating the behavior of different methods under various correlations, data are set to be uniformly distributed under the values of m_1 and a_1. For the comparison with baselines and variants, we introduce attribute correlations and hidden correlations by setting $p(a_2|m_1)$ to Table 11. For additional analysis, we introduce hidden correlations by setting $p(a_2|m_1)$ according to Table 12, where we set $corr_p = 0.5, 0.6, 0.7, 0.8, 0.9$ for hidden correlations $cor_h = 0, 0.02, 0.08, 0.19, 0.37$, respectively.

Time Series Leave-one-group-out validation is performed, where each group is selected as the test group once, and the remaining groups serve as the training groups. Groups are obtained by dividing the data by the value of attribute a_2, where the number of values of a_2 is equal for different groups. The training and validation sets are obtained by splitting the data of the training groups by 0.8:0.2. All data of the test group form the test set. All methods are trained on the training set, tuned on the validation set, and tested on the test set.

F.3 Implementation Details

We experiment with Pytorch 1.10.0+cu113 and Python 3.8.13. Model optimization is performed using Adam (Kingma & Ba, 2015). Experiments are conducted on Linux servers with Intel(R) Core(TM) i9-12900K CPUs and NVIDIA RTX 3090 GPUs.

Table 13: Hyper-parameter search spaces and NNI settings.

	Item	Search space / setting
Hyper-parameter	w_m	between [0.01, 10]
	S_d	[1, 3, 5, 7, 9]
	N_m	[2,3,4]
	l_c, l_d, l_e	[0.0001, 0.0003, 0.0005, 0.0007, 0.001]
NNI configuration	Max trial number per GPU	1
	Optimization algorithm	Tree-structured Parzen Estimator

G HYPER-PARAMETERS

The general hyper-parameters are set to the following values: The number of dimensions D for representations $\boldsymbol{z}_i$ is set to 128. The mini-batch size is set to 64 and 128 for toy and other datasets, respectively. The number of epochs for pre-training, E_1, and the number of epochs for supervised DRL, E_2, are set to 100 and 150, respectively. The numbers of update steps S_f and S_c are set to 1.

Some other hyper-parameters are tuned with Neural Network Intelligence (NNI)[1]. The search spaces and NNI configurations are given in Table 13. The tuned hyper-parameters are set to the following values: The weight of mode prediction loss w_m is set to 0.5, 0.2, 0.7, 0.1, 0.01, and 0.01 on toy, CMNIST, UCI-HAR, RealWorld, HHAR, and MFD for variants with mode prediction loss, respectively. The number of update steps S_d is set to 2, 15, 7, 7, 1, and 1 on toy, CMNIST, UCI-HAR, RealWorld, HHAR, and MFD, respectively. The number of modes N_m under each value of a_k is set to 3, 2, 8, 3, 2, and 2 on toy, CMNIST, UCI-HAR, RealWorld, HHAR, and MFD, respectively. The initial learning rates of Adam (l_c, l_d, l_e) are set to (0.001, 0.0007, 0.001), (0.001, 0.0003, 0.001), (0.001, 0.0007, 0.0005), (0.001, 0.001, 0.001), (0.001, 0.0001, 0.001), and (0.001, 0.001, 0.0005) on toy, CMNIST, UCI-HAR, RealWorld, HHAR, and MFD, respectively.

H BASELINES

We focus on comparing different independence constraints, and leave out the other components in the original baseline implementations, e.g., different architectures. For fair comparisons, all methods share the same encoder structure and train with alternative update steps, which is the same as SD-HC. The baselines are summarized below:

- **MMD** (Lin et al., 2020) minimizes the Maximum Mean Discrepancy between different distributions in the subspace of one attribute under different values of another attribute.
- **DTS** (Li et al., 2022) adversarially trains attribute predictors to make one attribute unpredictable from the representations of another.
- **IDE-VC** (Yuan et al., 2021) minimizes the unconditional MI between the representations of different attributes by adversarially training a predictor that predicts the representations of one attribute from those of another.
- **MI** (Cheng et al., 2022) and **A-CMI** (Funke et al., 2022) minimize the unconditional mutual information and the attribute-based conditional mutual information between the representations of different attributes, respectively. These two methods minimize MI by adversarially training an unconditional or conditional discriminator as the proposed method. We train two discriminators for A-CMI to minimize conditional mutual information based on both a_1 and a_2 as in (Funke et al., 2022).
- **HFS** minimizes the Hausdorff distance between two representation sets to factorize the supports of different representation subspaces, where we use Euclidean distance as the distance measure between different representations from the same subspace as in (Oublal et al., 2024).

[1] https://github.com/microsoft/nni

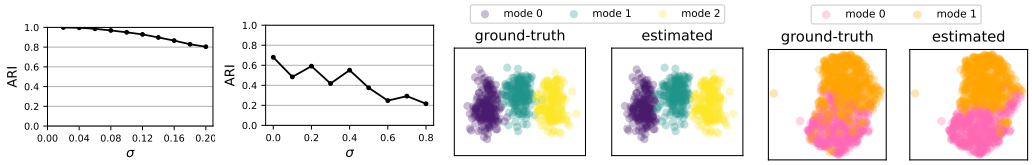

(a) ARI, toy (b) ARI, CMNIST (c) Clusters, toy (d) Clusters, MNIST

Figure 15: Clustering performance. (a) and (b) shows the ARI on toy and CMNIST under varying noise levels. (c) and (d) shows the true and estimated cluster assignments under $a_1 = 0$ on the raw toy data and the CMNIST representations of BASE by t-SNE(Maaten, L. V. D. and Hinton, G., 2008).

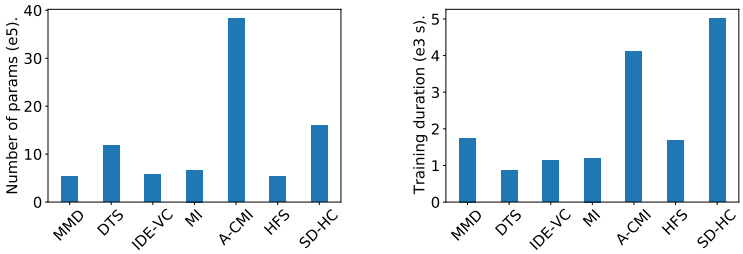

(a) Number of parameters (b) Training duration

Figure 16: Computational complexity comparison.

I Additional Model Investigation

Clustering Evaluation. We use adjusted rand index (ARI) to measure clustering performance. ARI ranges between 0 and 1, with 0 indicating a random cluster assignment, and 1 indicating a perfectly matching cluster assignment with ground truth. The results are shown in Figure 15ab, which shows that: (1) As the noise level increases, ARI drops due to information loss; (2) CMNIST shows lower ARI than toy, as real data are more challenging; (3) The high ARI under moderate noises indicates effective clustering, as validated by the similarity to true cluster assignments in Figure 15cd.

The clustering algorithm is a choice of design for our method. Although k-means has been effective across our experiments, we offer practical guidance regarding the alternative clustering methods that could be considered for real applications. For high-dimensional data, Marigold (Mortensen et al., 2023) could be considered, which is an extension of k-means to high-dimensional cases. For more complex data, deep clustering (Ronen et al., 2022) could be considered, which can make representation learning and clustering mutually enhance each other by alternative training. Self-supervised learning (Zhang et al., 2019) could also be incorporated to improve the quality of representations for complex data.

Computational Complexity Figure 16 shows the total numbers of parameters and the training durations of a single leave-one-group-out validation process (without repetition) on UCI-HAR of SD-HC and the compared methods.

In Figure 16a, we observe that A-CMI has the most parameters, which is because A-CMI has two discriminators for minimizing conditional mutual information based on a_1 and a_2. This indicates that our method is computationally efficient w.r.t. number of parameters compared to A-CMI, which is advantageous for deployment in resource-constrained environments.

In Figure 16b, we observe that the training durations of A-CMI and SD-HC are the longest. This is because within one mini-batch, the number of samples under one mode value is much smaller than those under one attribute value, and we find that SD-HC needs more update steps to sufficiently learn the discriminator. Therefore, in real applications, the better approach is to upload the data to the server for training, and then locally download the trained network for inference.

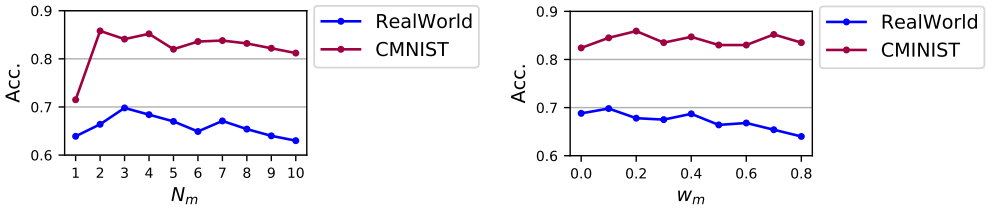

(a) N_m (b) w_m

Figure 17: Hyper parameter sensitivity experiments of (a) N_m and (b) w_m .

Table 14: Results on MINIST dataset. "*" indicates that SD-HC is statistically superior to the compared method according to the pairwise t-test at a 95% significance level. The results of the best methods are **bold**. The result of the best baseline DRL methods are underlined, over which the improvement achieved by SD-HC is calculated.

Method	Test 1 (correlated)		Test 2 (uncorrelated)		Test 3 (anticorrelated)	
	Acc.	Mac. F1	Acc.	Mac. F1	Acc.	Mac. F1
BASE	**0.901** ±0.003	**0.901** ±0.003	0.831 ±0.003	0.831 ±0.003	0.768 ±0.008	0.768 ±0.008
MMD	0.640 ±0.114	0.589 ±0.160	0.614 ±0.088	0.562 ±0.133	0.582 ±0.069	0.528 ±0.117
DTS	0.699 ±0.041	0.699 ±0.041	0.651 ±0.029	0.651 ±0.029	0.615 ±0.022	0.615 ±0.022
IDE-VC	0.632 ±0.031	0.629 ±0.031	0.588 ±0.025	0.585 ±0.028	0.539 ±0.022	0.533 ±0.027
MI	0.664 ±0.018	0.660 ±0.018	0.628 ±0.019	0.624 ±0.019	0.596 ±0.014	0.590 ±0.018
A-CMI	0.722 ±0.072	0.712 ±0.081	0.668 ±0.049	0.658 ±0.058	0.611 ±0.039	0.600 ±0.044
HFS	0.811 ±0.014	0.809 ±0.014	0.725 ±0.012	0.723 ±0.012	0.635 ±0.008	0.631 ±0.008
SD-HC (ours)	0.886 ±0.005	0.886 ±0.008	**0.859** ±0.009	**0.859** ±0.010	**0.829** ±0.011	**0.829** ±0.008
Improvement	↓1.5	↓1.5	↑2.8 %	↑2.8 %	↑6.1 %	↑6.1 %

Parameter Sensitivity of N_m. The sensitivity to the number of modes N_m under each attribute value is shown in Figure 17a, which shows that: (1) SD-HC performs the best at the ground truth $N_m = 2$ on CMNIST, suggesting that prior knowledge about N_m would be beneficial. (2) SD-HC performs badly at $N_m = 1$, where mode-based CMI degrades to attribute-based CMI, causing the loss of mode information. (3) In general, SD-HC is not particularly sensitive to changes of N_m within a certain range. On CMNIST, SD-HC performs comparably under $N_m = 2, 3, 4$, suggesting that SD-HC is robust to the changes of N_m when it is slightly larger than the ground truth ($N_m = 2$). Probably because as long as the samples within one estimated cluster belong to the same ground-truth mode, SD-HC can preserve mode information to some extent.

In practice, hyper-parameter tuning may come with high computational costs for large-scale datasets. Alternatively, we offer practical guidance to reduce the computational costs by estimating the number of modes N_m in a data-driven manner. This requires expert knowledge to choose the suitable method: For well-separated clusters, Elbow Method (Marutho et al., 2018) would be suitable for estimating N_m with k-means clustering; For complex and overlapping clusters, Bayesian Information Criterion (Watanabe, 2013) would be suitable for estimating N_m with Gaussian Mixture Models for clustering; In addition, during our pre-training stage, the number of modes can be estimated by split and merge operations with deep clustering methods (Ronen et al., 2022).

Parameter Sensitivity of w_m. The sensitivity to the weight parameter of mode prediction loss, w_m, is shown in Figure 17b, which shows that: In general, SD-HC performs better at a small value of w_m. Theoretically, adding mode prediction loss benefits disentanglement. However, enforcing mode prediction with estimated mode labels will potentially introduce errors, as the estimated mode labels do not match the ground-truth mode labels.

J Full Results on CMNIST Dataset

The full comparison with baselines on CMNIST dataset is presented in Table 14, from which we observe that the advantage of SD-HC increases as correlation shift increases from test 1 to test 3.